Goethe-Universität Frankfurt am Main

Institut für Theoretische Physik

# Determination of $\Lambda_{\overline{MS}}$ from the static quark-antiquark potential in momentum space

Masterarbeit

*eingereicht von:*
Antje Peters

*Betreuer und Erstgutachter:*
Prof. Dr. Marc Wagner

*Zweitgutachter:*
Dr. Felix Karbstein



März 2014

This work deals with the determination of the scale parameter $\Lambda_{\overline{MS}}$ from lattice QCD and perturbation theory results of the static quark-antiquark potential for $n_f = 2$. The investigation is done in momentum space. Lattice methods as well as perturbation theory calculations are introduced. Another part of this work concerns the calculation of the quark-antiquark potential from gauge link configurations for $n_f = 2 + 1 + 1$.

# Contents

# 1. Introduction

## 1.1. Strong interaction

Quarks are the building blocks of matter. Hadrons, like the proton and the neutron, are composed of them. Quarks come in 6 different masses. Protons and neutrons are build of rather light up and down quarks. More exotic particles, that for example can be created in particle accelerators, are also composed of strange, charm, bottom and top quarks. In a calculation $n_f$ denotes the number of quark flavours. To describe a process that involves quarks one should actually consider six quark flavours with six different masses. Because those calculations would be extremely elaborate and time-consuming, one inspects models with less flavours to approximate reality. For example a model with $n_f = 2$ means to consider only the two lightest quark flavours (up quark and down quark) which are assumed to have the same mass in this case. $n_f = 2 + 1 + 1$ denotes two quark flavours of the same mass plus a heavier one (strange quark) plus one even heavier one (charm quark). The quark regime is ruled by the strong interaction. The quantum theory of the strong interaction is called quantum chromodynamics (QCD). Strong interaction affects particles (like quarks) that feature a quantum number called colour charge. Colour charge is different from electromagnetic charge: There are three different states and each of them has an anti-state. One calls those "colours" (anti-)red, (anti-)blue and (anti-)green: $\overline{r}, r$; $\overline{b}, b$; $\overline{g}, g$. The messenger that submits information between quarks, the strong interaction, is called the gluon. The gluon is colour charged by a combination of colour and anti-colour. There are 8 linearly independent combinations, so gluons appear in 8 different states.

Because of their charge, gluons interact. The interaction is responsible for the different behaviour of electromagnetic and strong interaction. While electrons that are subject to the electromagnetic force can be separated with a little support of energy, this is (with our known instruments) not possible for quarks. This phenomenon is called *confinement*.

The attractive potential energy between a quark and an antiquark is subject of particular interest for physicists because it provides information about the sub-nuclear world. To calculate it one has to solve path integrals that contain the action of QCD. The action contains terms beyond quadratic order, so the integrals cannot be solved exactly analytically. For this reasons different approaches have to be taken to learn about QCD.

## 1.2. Lattice QCD and perturbation theory

As mentioned in the previous section, there is no way to solve QCD path integrals exactly analytically. There are several ways to deal with this problem. One way is to choose the perturbative approach and solve the path integrals by a series expansion in orders of the coupling constant $\alpha_s$. This method is only reliable, if the coupling is small enough. This is the case in high energy reactions, when the interaction of the involved particles is weak. The perturbative calculations used in this work will be described in detail in chapter 2.

In the low-energy regime the coupling parameter of QCD becomes large. In this case one needs to describe QCD with non-perturbative methods. In the 1970s, Kenneth Wilson proposed the lattice QCD as an adequate theory based on discretized Euclidean space-time which avails itself of techniques from statistical physics [1]. Theoretically, the lattice approach is able to describe physics reliably in the high- as well as in the low-energy regime. Technically, lattice computations are limited by the lattice spacing and extent. So lattice QCD can describe the quark-antiquark potential at separations, which are large in comparison to the lattice spacing, but small compared to the lattice extend, otherwise lattice errors predominate.

Effectively, both approaches describe the same physics at different energies. The difficulty is to match them in an energy range where both theories overlap.

## 1.3. Motivation: The parameter $\Lambda_{\overline{MS}}$

The parameter $\Lambda$ with dimension energy is a convenient choice to define a reference momentum scale in perturbation theory. On the other hand, the Sommer parameter $r_0$ defines the scale in lattice QCD (cf. chapter 3). A result without a scale has no physical meaning. In order to identify the scale, the quantity $\Lambda r_0$ can be determined. To that purpose, one needs to describe a physical observable both on the lattice and with the perturbative approach and, as done in this work, solve for $\Lambda$, if $r_0$ is known. The quark-antiquark potential is a suitable observable because there is a sufficiently quick way to compute it on the lattice and it is precisely analysed in perturbation theory. If the calculations are done in the $\overline{MS}$-renormalization scheme (modified Minimal Subtraction Scheme), the energy scale is called $\Lambda_{\overline{MS}}$ [2].

### 1.3.1. Determination of $\Lambda_{\overline{MS}}$ in position space

In 2011 $\Lambda_{\overline{MS}}$ was already determined by comparison of the perturbative potential with lattice data for $n_f = 2$ [3]. The comparison of lattice QCD and perturbation theory results was done in position space. The result

$$\Lambda_{\overline{MS}} = 315(30)\text{MeV} \tag{1.1}$$

was obtained. Lattice theory is usually done in position space and perturbation theory is done in momentum space for convenience. So the idea was to Fourier-transform perturbation theory results to position space before the comparison to lattice results. The problem was that perturbation theory is wrong for momentum transfers $< \Lambda\,(\approx 300$ MeV). So the Fourier transform

$$V_{pert}(r) = \int \frac{\mathrm{d}^3 p}{(2\pi)^3} \mathrm{e}^{i\vec{p}\cdot\vec{r}} \tilde{V}_{pert}(p) \tag{1.2}$$

has a systematic error.

In the hope of finding a more precise result for $\Lambda_{\overline{MS}}$ the new idea formulated in this work is to get the potential in momentum space directly from perturbation theory and consider it only for sufficiently large momenta. This time the lattice results are transformed to momentum space, which means that a discrete Fourier transform (DFT) is applied to a list of lattice data. The systematic error due to considering perturbation theory in an inappropriate momentum range does not occur anymore. In summary, the aim of this work is to reduce the error, which was determined according to the former result, by the application of this momentum space-approach.

# 2. Perturbation theory

Since QCD deals with strongly interacting quarks and gluons, it is described by the SU(3) component of the standard model of physics. The aim of perturbation theory is to solve problems of QCD analytically. Its physical limit is the increase of the coupling parameter $\alpha_s$ at small momentum transfers.

## 2.1. The renormalized coupling $\alpha_s$

The parameter of perturbation theory in QCD, besides the quark masses, is the coupling parameter $\alpha_s$, $s$ for *strong interaction*. $\alpha_s$ depends on a dimensionful renormalization scale $\mu$ which has no immediate physical impact. By choosing a scale in the order of the momentum transfer in the considered process $\alpha_s(\mu)$ denotes the interaction strength in the process. Because of the scale dependence $\alpha_s(\mu)$ is referred to as running coupling. The explicit value of $\alpha_s(\mu)$ is not independent of the renormalizaton *scheme* it is evaluated in. A renormalization scheme is necessary to relate observables computed in lattice simulations or perturbative calculations to phenomenology. The most common scheme is the already mentioned Modified Minimal Subtraction scheme ($\overline{MS}$) [2,4].

Evaluations presented in this work refer to $\overline{MS}$.

## 2.2. Formula from perturbation theory used in this work

One of the challenges of perturbation theory is to compute the static quark-antiquark potential order by order in $\alpha_s(\mu)$ analytically. The computation is done in momentum space.

Conventionally, the static potential has the form [3,5]:

$$\tilde{V}(p) = V_0 - C_F \frac{4\pi}{p^2} \tilde{\alpha_V}[\alpha_s(\mu), L(\mu, p)] \tag{2.1}$$

with

$$L(\mu, p) = \ln \frac{\mu^2}{p^2} \equiv L \tag{2.2}$$

$V_0$ is a constant energy offset. In the gauge group SU(3) in the fundamental representation the eigenvalue of the quadratic Casimir operator is $C_F = \frac{4}{3}$.

The most logic action now would be to expand the potential respectively $\tilde{\alpha_V}$ in powers of the coupling $\alpha_s$. But the calculation is more complicated [6,7] since thousands of diagrams have to be considered. In higher orders a strict power series expansion breaks down and there are also logarithmic terms in $\alpha_s$ [8]. The following terms are known explicitly:

$$\begin{aligned} \tilde{\alpha_V}[\alpha_s(\mu), L(\mu, p)] =& \alpha_s(\mu) \Big\{ 1 + \frac{\alpha_s(\mu)}{4\pi} P_1(L) + \left( \frac{\alpha_s(\mu)}{4\pi} \right)^2 P_2(L) \\ &+ \left( \frac{\alpha_s(\mu)}{4\pi} \right)^3 [P_3(L) + a_{3\ln} \ln \alpha_s(\mu)] + ... \Big\} \end{aligned} \tag{2.3}$$

The coefficients $P_1, P_2, P_3$ and $a_{3\ln}$ can be found in appendix A. For convenience the terms of linear order in $\alpha_s(\mu)$ in the following are referred to as leading order (LO), up to $\mathcal{O}(\alpha_s(\mu)^2)$ as next-to-leading order (NLO), up to $\mathcal{O}(\alpha_s(\mu)^3)$ as next-to-next-to-leading order (NNLO) and $\mathcal{O}(\alpha_s(\mu)^4)$ as well as $\mathcal{O}(\alpha_s(\mu)^4 \ln \alpha_s(\mu))$ as next-to-next-to-next-to-leading order (NNNLO).

On the other hand since the scale $\mu$ is not physical, a physical observable must not depend of this scale explicitly. One says, the potential is a renormalization group invariant and one can require:

$$\mu \frac{\mathrm{d}}{\mathrm{d}\mu} \tilde{\alpha_V}[\alpha_s(\mu), L(\mu, p)] \stackrel{!}{=} 0 \tag{2.4}$$

This condition should hold for all orders of $\alpha_s(\mu)$. Since the potential is not known beyond $\mathcal{O}(\alpha_s(\mu)^4)$, one actually has:

$$\mu \frac{\mathrm{d}}{\mathrm{d}\mu} \tilde{\alpha_V}[\alpha_s(\mu), L(\mu, p)] = \mathcal{O}(\alpha_s(\mu)^5) \tag{2.5}$$

As described in [9] and using a series expansion of (2.1) this can be converted to

$$\left( \frac{\partial}{\partial L} + \frac{\alpha_s(\mu)}{2} \beta[\alpha_s(\mu)] \frac{\partial}{\partial \alpha_s(\mu)} \right) \tilde{\alpha_V}[\alpha_s(\mu), L(\mu, p)] = 0 \tag{2.6}$$

with the QCD $\beta$-function

$$\beta[\alpha_s(\mu)] = \frac{\mu}{\alpha_s(\mu)} \frac{d\alpha_s(\mu)}{\mathrm{d}\mu} \tag{2.7}$$

which again can be expanded in $\alpha_s(\mu)$:

$$\beta[\alpha_s(\mu)] = -\frac{\alpha_s(\mu)}{2\pi} \sum_{n=0}^{\infty} \left( \frac{\alpha_s(\mu)}{4\pi} \right)^n \beta_n \tag{2.8}$$

The coefficients $\beta_0$ up to $\beta_3$ are known. The numerical values can be found in appendix A.
One can expand $\alpha_s(\mu)$ in orders of $\alpha_s(\nu)$:

$$\begin{aligned} \alpha_s(\mu) =& \alpha_s(\nu) \Big[ 1 - \frac{\alpha_s(\nu)}{4\pi} \beta_0 \ln \frac{\mu^2}{\nu^2} + \left( \frac{\alpha_s(\nu)}{4\pi} \right)^2 \left( \beta_0^2 \ln \frac{\mu^2}{\nu^2} - \beta_1 \right) \ln \frac{\mu^2}{\nu^2} \\ & - \left( \frac{\alpha_s(\nu)}{4\pi} \right)^3 \left( \beta_0^3 \ln^2 \frac{\mu^2}{\nu^2} - \frac{5}{2} \beta_0 \beta_1 \ln \frac{\mu^2}{\nu^2} + \beta_2 \right) \ln \frac{\mu^2}{\nu^2} \Big] + \mathcal{O}(\alpha_s(\nu)^5) \end{aligned} \tag{2.9}$$

This equation fulfils equations (2.7) and (2.8).

As an expansion parameter $\alpha_s$ must be small for any momentum scale, i.e. $\alpha_s(\nu), \alpha_s(\mu) \ll 1$. This requirement guarantees $\mu$ and $\nu$ to be in the same order of magnitude, which prevents the logarithms in (2.9) from becoming large.

One can easily see, that insertion of (2.9) into equation (2.3) yields the same expressions as before, replacing $\mu$ by $\nu$. This confirms, that the scale $\mu$ in fact is only a parameter that can be substituted by another.

It it easy to switch to another scale because the relation $\alpha_s(\mu) = f[\alpha_s(\nu)]$ is known. Under the constraints mentioned above, one is free to choose the most convenient parameter.

On the other hand this allows the inspection that there is no physical constraint to discover the renormalization scale subjected to a natural energy scale. Not until the integration of (2.7) one finds a reference parameter. One possible definition is $\Lambda_{\overline{MS}}$. There are different ways to compute the integral differing in how many orders of the series expansion of the $\beta$-function and of $\alpha_s(\mu)$ are considered and at which point a numerical calculation is applied. Starting point is equation (2.7).

The easiest way is to integrate only considering the leading order ($n = 0$) with $\beta[\alpha_s(\mu)] = -\frac{\alpha_s(\mu)}{2\pi} \beta_0$, which yields:

$$
\begin{aligned}
-\frac{\alpha_s(\mu)}{2\pi}\beta_0 &= \frac{\mu}{\alpha_s(\mu)}\frac{\mathrm{d}\alpha_s(\mu)}{\mathrm{d}\mu} \\
\Rightarrow -\frac{\beta_0}{2\pi}\int_\mu^{\Lambda_{\overline{MS}}}\frac{1}{\mu'}\mathrm{d}\mu' &= \int_{\alpha_s(\mu)}^{\infty}\frac{1}{\alpha_s(\mu')^2}\mathrm{d}\alpha_s(\mu') \\
\Rightarrow \qquad \Lambda_{\overline{MS}} &= \mu \mathrm{e}^{-\frac{2\pi}{\beta_0\alpha_s(\mu)}}
\end{aligned}
\tag{2.10}
$$

As a boundary condition $\alpha_s(\mu)$ vanishes because of asymptotic freedom. One can easily understand the meaning of $\Lambda_{\overline{MS}}$:

$$
\mu = \Lambda_{\overline{MS}} \qquad \Longrightarrow \quad \alpha_s(\mu) = \infty \tag{2.11}
$$

Which means that perturbation theory is only reliable if $\mu \gg \Lambda_{\overline{MS}}$.

Taking into account higher orders of (2.7) and (2.8) yields (cf. e.g. [3]):

$$
\begin{aligned}
\Lambda_{\overline{MS}} &= \mu\left(\frac{\beta_0\alpha_s(\mu)}{4\pi}\right)^{-\frac{\beta_1}{2\beta_0^2}} \exp\left(-\frac{2\pi}{\beta_0\alpha_s(\mu)} - \int_0^{\alpha_s(\mu)}\frac{\mathrm{d}\alpha_s'}{\alpha_s'}\left(\frac{1}{\beta[\alpha_s']} + \frac{2\pi}{\beta_0\alpha_s'} - \frac{\beta_1}{2\beta_0^2}\right)\right) \\
\Rightarrow \ln\left(\frac{\mu}{\Lambda_{\overline{MS}}}\right) &= \ln\left(\frac{\beta_0\alpha_s(\mu)}{4\pi}\right)^{\frac{\beta_1}{2\beta_0^2}} + \frac{2\pi}{\beta_0\alpha_s(\mu)} + \int_0^{\alpha_s(\mu)}\frac{\mathrm{d}\alpha_s'}{\alpha_s'}\left(\frac{1}{\beta[\alpha_s']} + \frac{2\pi}{\beta_0\alpha_s'} - \frac{\beta_1}{2\beta_0^2}\right)
\end{aligned}
\tag{2.12}
$$

Inserting the whole known series expansion of the $\beta$-function (2.7) into (2.12) yields:

$$
\begin{aligned}
\ln\left(\frac{\mu}{\Lambda_{\overline{MS}}}\right) =& \ln\left(\frac{\beta_0\alpha_s(\mu)}{4\pi}\right)^{\frac{\beta_1}{2\beta_0^2}} + \frac{2\pi}{\beta_0\alpha_s(\mu)} \\
&+ \int_0^{\alpha_s(\mu)}\frac{\mathrm{d}\alpha_s'}{\alpha_s'}\left(\frac{-2\pi}{\alpha_s'\left(\beta_0 + \frac{\alpha_s'}{4\pi}\beta_1 + \left(\frac{\alpha_s'}{4\pi}\right)^2\beta_2 + \left(\frac{\alpha_s'}{4\pi}\right)^3\beta_3\right)} + \frac{2\pi}{\beta_0\alpha_s'} - \frac{\beta_1}{2\beta_0^2}\right)
\end{aligned}
\tag{2.13}
$$

A Taylor series expansion of the first summand of the integrand in leading order yields:

$$
\begin{aligned}
\frac{-2\pi}{{\alpha_s'}^2\left(\beta_0 + \frac{\alpha_s'}{4\pi}\beta_1 + \left(\frac{\alpha_s'}{4\pi}\right)^2\beta_2 + \left(\frac{\alpha_s'}{4\pi}\right)^3\beta_3\right)} =& -\frac{2\pi}{\beta_0{\alpha_s'}^2} + \frac{\beta_1}{2\beta_0^2\alpha_s'} - \frac{\beta_1^2 - \beta_0\beta_2}{8\pi\beta_0^3} \\
&+ \frac{\beta_0^2\beta_3 - 2\beta_0\beta_1\beta_2 + \beta_1^3}{32\pi^2\beta_0^4}\alpha_s' + \mathcal{O}({\alpha_s'}^2)
\end{aligned}
\tag{2.14}
$$

Performing the $\mathrm{d}\alpha_s'$ integral yields:

$$
\begin{aligned}
\int_0^{\alpha_s}\mathrm{d}\alpha_s'\frac{-2\pi}{{\alpha_s'}^2\left(\beta_0 + \frac{\alpha_s'}{4\pi}\beta_1 + \left(\frac{\alpha_s'}{4\pi}\right)^2\beta_2 + \left(\frac{\alpha_s'}{4\pi}\right)^3\beta_3\right)} =& \left[\frac{4\pi}{\beta_0\alpha_s'} + \frac{\beta_1}{2\beta_0^2}\ln\alpha_s' - \frac{\beta_1^2 - \beta_0\beta_2}{8\pi\beta_0^3}\alpha_s'\right. \\
&\left. + \frac{\beta_0^2\beta_3 - 2\beta_0\beta_1\beta_2 + \beta_1^3}{64\pi^2\beta_0^4}{\alpha_s'}^2 + \mathcal{O}({\alpha_s'}^3)\right]_0^{\alpha_s(\mu)}
\end{aligned}
\tag{2.15}
$$

Applying this expression to (2.13) leads to [1]:

[1] Note that the $\frac{1}{\alpha_s'}$- and $\ln\alpha_s'$-terms of the primitive cancel, so the lower integral border 0 causes no difficulties.

$$\ln\left(\frac{\mu}{\Lambda_{\overline{MS}}}\right) = \frac{2\pi}{\beta_0\alpha_s(\mu)} + \frac{\beta_1}{2\beta_0^2}\ln\left(\frac{\beta_0\alpha_s(\mu)}{4\pi}\right) + \frac{\beta_0\beta_1-\beta_1^2}{8\pi\beta_0^3}\alpha_s(\mu) + \frac{\beta_0^2\beta_3-2\beta_0\beta_1\beta_2+\beta_1^3}{64\pi^2\beta_0^4}\alpha_s(\mu)^2 \tag{2.16}$$

Inserting the numerical coefficients into (2.12) leads to the equation:

$$\begin{aligned}\ln\left(\frac{\mu}{\Lambda_{\overline{MS}}}\right) =& \ln\left[\frac{5.03839\alpha_s(\mu)^{\frac{345}{841}}}{(12.5664\alpha_s(\mu)+12.9623)^{\frac{543062567}{2000000000}}\left((12.5664\alpha_s(\mu)-2.32775)^2+167.502\right)^{0.0693473}}\right] \\ &+ \frac{0.649985}{\alpha_s(\mu)} - 0.3841\arccos\left(\frac{12.5664\alpha_s(\mu)-2.32775}{\sqrt{(12.5664\alpha_s(\mu)-2.32775)^2+167.502}}\right)\end{aligned} \tag{2.17}$$

To derive $\Lambda_{\overline{MS}}$ from the static potential, the expression (2.3) is inserted into (2.1). The expression is fitted to the lattice potential in momentum space. Notice that the fit function has two degrees of freedom: $\alpha_s$ and an additional fitting parameter $\tilde{V}_0$.

The fit result for $\alpha_s$ is applied to (2.16) and (2.17). $\mu$ is chosen in the order of magnitude of the momentum transfer. The formulae are solved for $\Lambda_{\overline{MS}}$.

To compute $\alpha_s(\mu)$ explicitly as a function of $\ln\frac{\mu^2}{\Lambda^2_{\overline{MS}}}$, $\alpha_s(\mu)$ is expanded in orders of $\ln\frac{\mu^2}{\Lambda^2_{\overline{MS}}}$ and the expression (2.16) is iteratively solved [3, 10]:

$$\begin{aligned}\alpha_s(\mu) =& \frac{4\pi}{\beta_0 l}\left\{1 - \frac{\beta_1}{\beta_0^2 l}\ln l + \left(\frac{\beta_1}{\beta_0\beta_0 l}\right)^2\left[\ln^2 l - \ln l - 1 + \frac{\beta_0\beta_2}{\beta_1^2}\right]\right. \\ &\left. - \left(\frac{\beta_1}{\beta_0^2 l}\right)^3\left[\ln^3 l - \frac{5}{2}\ln^2 l - \left(2 - \frac{3\beta_0\beta_2}{\beta_1^2}\right)\ln l + \frac{1}{2}\left(1 - \frac{\beta_0^2\beta_3}{\beta_1^3}\right)\right]\right\}\end{aligned} \tag{2.18}$$

$$\text{with} \qquad l = \ln\frac{\mu^2}{\Lambda^2_{\overline{MS}}} \tag{2.19}$$

Using this equation, $\Lambda_{\overline{MS}}$ can be extracted directly from a fit of (2.1) to lattice data.

Briefly, the following equations are considered to determine $\Lambda_{\overline{MS}}$:

**(2.16)** : An equation for $\Lambda_{\overline{MS}}$ that depends on $\alpha_s(\mu)$. To derive the equation, one Taylor series expansion in $\alpha_s(\mu)$ is applied in equation (2.12) in order to solve the integral.

**(2.17)** : A similar equation for $\Lambda_{\overline{MS}}$, but this time the integral in (2.12) is solved numerically. Since equations (2.16) and (2.17) should provide similar results they can be used to cross check the algorithms of the lattice computations.

**(2.18)** : An explicit equation for $\alpha_s(\mu)$. $\Lambda_{\overline{MS}}$ can be determined by a direct fit to lattice data. To derive the equation, both a Taylor series expansion in $\alpha_s(\mu)$ and a series expansion in $\ln\frac{\mu^2}{\Lambda^2_{\overline{MS}}}$ is applied.

# 3. Computation of the quark-antiquark potential on the lattice

In this chapter lattice techniques are introduced using the example of the static quark-antiquark potential. The potential is computed for $n_f = 2 + 1 + 1$. The computation is done to determine $r_0$ and set the scale of a set of configurations recently generated by the ETMC[1]. Further analysis will be done elsewhere in the future. The determination of $\Lambda_{\overline{MS}}$ described in chapter 4 is based on a potential for $n_f = 2$ that had already been calculated in the context of [3]. However, the methods used for calculating the potential are the same regardless of how many dynamical quark flavours are considered. The basic theoretical concepts follow [11].

## 3.1. Lattice parameters

The parameters of a lattice calculation are the coupling constant $\beta$, the quark masses, the lattice spacing $a$ and the lattice extension $L$ in space and $T$ in time:

$$L = N_L a \qquad T = N_T a \qquad \text{with} \quad N_L, N_T \in \mathbb{N} \tag{3.1}$$

A lattice quark field can be understood as a lattice site. The lattice spacing can be pictured as the distance between two lattice sites (cf. figure 3.1).

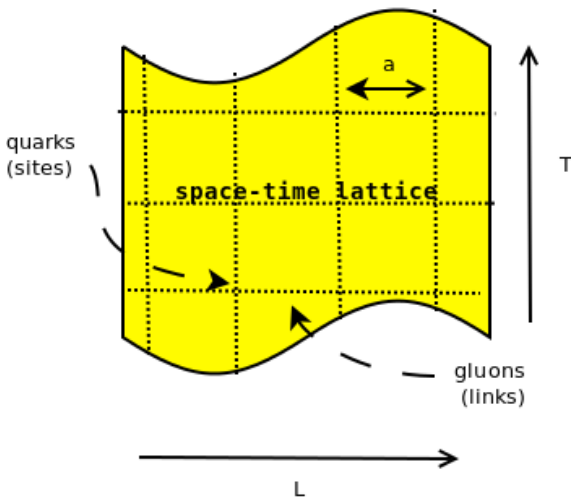


Figure 3.1.: A space-time lattice sketched in two dimensions

Since QCD is described by the colour gauge group SU(3), a quark field $Q$ transforms with $V(x) \in \mathrm{SU}(3)$:

$$Q(x) \to Q'(x) = V(x)Q(x) \tag{3.2}$$

$$\overline{Q}(x) \to \overline{Q}'(x) = \overline{Q}(x)V^\dagger(x) \tag{3.3}$$

[1] European Twisted Mass Collaboration

with $x = (\vec{x}, \tau)$ a four-vector in Euclidean space-time. A lattice gluon field is a lattice link. It is an element of SU(3) itself. Let $\hat{\mu}$ be the unit vector in direction $\mu$. A gluon field $U$ transforms like:

$$U_\mu(x) \to U'_\mu(x) = V(x)U_\mu(x)V^\dagger(x + a\hat{\mu}) \tag{3.4}$$

## 3.2. The quark-antiquark potential: determination

To determine the quark-antiquark potential, consider the case of infinitely heavy quarks at fixed positions. Those quarks can neither be created nor annihilated, they simply exist. The potential $V_{Q\overline{Q}}(r)$ between those quarks is the energy difference between the QCD vacuum state $|\Omega\rangle$ and the least excited state that contains one quark-antiquark pair with the spacial distance $r$. A quark-antiquark state $|\Phi\rangle$ can be described by the operator

$$O_{Q\overline{Q}}(r) = \overline{Q}(\vec{x})U(\vec{x}, \vec{y})Q(\vec{y}) \tag{3.5}$$

with $r = |\vec{x} - \vec{y}|$ and $U(\vec{x}, \vec{y})$ the product of all links between the spacial points $\vec{x}$ and $\vec{y}$ and

$$|\Phi(r)\rangle = O_{Q\overline{Q}}(r)\,|\Omega\rangle \tag{3.6}$$

The behaviour of the quark-antiquark state over an Euclidean time $\tau$ can be described by the correlation function

$$\begin{aligned}
\mathcal{C}(r,\tau) &= \langle\Omega|\, O^\dagger_{Q\overline{Q}}(r)\mathrm{e}^{-H\tau}O_{Q\overline{Q}}(r)\mathrm{e}^{+H\tau}\,|\Omega\rangle \\
&= \sum_n \langle\Omega|\, O^\dagger_{Q\overline{Q}}(r)\mathrm{e}^{-H\tau}\,|n\rangle\,\langle n|\, O_{Q\overline{Q}}(r)\mathrm{e}^{+H\tau}\,|\Omega\rangle \\
&= \sum_n \langle\Phi(r)\,|\,n\rangle\,\langle n\,|\,\Phi(r)\rangle\,\mathrm{e}^{-(E_n(r)-E_\Omega)\tau} \\
&= \sum_n |\,\langle\Phi(r)\,|\,n\rangle\,|^2\mathrm{e}^{-(E_n(r)-E_\Omega)\tau}
\end{aligned} \tag{3.7}$$

Here states are expressed in the Heisenberg picture and in the third step a complete set of energy eigenstates is inserted. Take a look at equation (3.7). For large $\tau$ higher excited energy states are suppressed. The only summand that contributes is the one corresponding to the ground state $|0\rangle$:

$$\lim_{\tau\to\infty}\mathcal{C}(r,\tau) = \lim_{\tau\to\infty}\sum_n |\,\langle\Phi(r)\,|\,n\rangle\,|^2\mathrm{e}^{-(E_n(r)-E_\Omega)\tau} = |\,\langle\Phi(r)\,|\,0\rangle\,|^2\mathrm{e}^{-(E_0(r)-E_\Omega)\tau} \tag{3.8}$$

And for the quark-antiquark potential one finds:

$$\begin{aligned}
V_{Q\overline{Q}}(r) &= \lim_{\tau\to\infty}\frac{1}{\Delta\tau}\underbrace{\ln\frac{\mathcal{C}(r,\tau)}{\mathcal{C}(r,\tau+\Delta\tau)}}_{V_{\mathrm{eff}(r,\tau)}} \\
&= \frac{1}{\Delta\tau}\ln\frac{|\,\langle\Phi(r)\,|\,0\rangle\,|^2\mathrm{e}^{-(E_0(r)-E_\Omega)\tau}}{|\,\langle\Phi(r)\,|\,0\rangle\,|^2\mathrm{e}^{-(E_0(r)-E_\Omega)(\tau+\Delta\tau)}} \\
&= \frac{1}{\Delta\tau}\ln\mathrm{e}^{(E_0(r)-E_\Omega)(\tau+\Delta\tau-\tau)} \\
&= \frac{1}{\Delta\tau}\ln\mathrm{e}^{(E_0(r)-E_\Omega)\Delta\tau} \\
&= E_0(r) - E_\Omega
\end{aligned} \tag{3.9}$$

$V_{\mathrm{eff}}$ is called the effective quark-antiquark potential.

To actually compute the quark-antiquark potential, further considerations are necessary.

The correlation function can be expressed as a function of the vacuum expectation value (VEV) of the so called Wilson loop $W_C[A]$

$$W(r,\tau) = \langle W_C[A] \rangle \tag{3.10}$$

with $A_\mu$ a gauge field. For large $\tau$, one can identify

$$\lim_{\tau\to\infty} W(r,\tau) = F(r)\mathrm{e}^{-E_0(r)\tau} \tag{3.11}$$

with $F(r)$ the overlap of the quark-antiquark state with the ground state. Compare to equation (3.8): In order to determine the quark-antiquark potential, one has to compute the VEV of the Wilson Loop and solve for the quark-antiquark potential:

$$V_{Q\overline{Q}}(r) = E_0(r) - E_\Omega = -\lim_{\tau\to\infty} \frac{1}{\tau} \ln \frac{W(r,\tau)}{W(r,\tau+\Delta\tau)} \tag{3.12}$$

### 3.2.1. Calculations on the lattice

As mentioned above, the aim is to compute the VEV of the Wilson loop. On the lattice, the Wilson loop takes a simple form:

$$W_C[U] = Tr \prod_{l\in C_L} U_l \tag{3.13}$$

with

$$\prod_{l\in C_L} U_l = U(n,m)_{C_L} \tag{3.14}$$

$n$ and $m$ are the lattice sites that correspond to one space-time point each which are connected by a path $C_L$. $U_l$ denotes a lattice link along $C_L$. The VEV of the Wilson loop reads:

$$W(R,T) = \langle W_C[U] \rangle = \frac{1}{Z} \int \mathrm{D}\chi\mathrm{D}\overline{\chi}\mathrm{D}U \exp[-S[\chi,\overline{\chi},U]] W_C[U] \tag{3.15}$$

This path integral can be treated as follows:
Any physical observable $O$ can be calculated as VEV $\langle O \rangle$. In the path integral formalism for $n_f = 2$ the VEV takes the form

$$\langle O \rangle = \langle \Omega | \, T\{O(\chi,\overline{\chi},U)\} \, | \Omega \rangle = \frac{1}{Z} \int \mathrm{D}\chi\mathrm{D}\overline{\chi}\mathrm{D}U \exp[-S[\chi,\overline{\chi},U]] O(\chi,\overline{\chi},U) \tag{3.16}$$

with $Z = \int \mathrm{D}\chi\mathrm{D}\overline{\chi}\mathrm{D}U \exp[-S[\chi,\overline{\chi},U]]$. $T$ denotes the time-ordered product.
$S[\chi,\overline{\chi},U] = S_F[\chi,\overline{\chi}] + S_G[U]$ is the action. The gauge part of the action is tree-level Symanzik improved [12]:

$$S_G[U] = \frac{\beta}{6} \left( b_0 \sum_{x\neq y} \mathrm{Tr}\left(1 - U^{1\times1}(x,y)\right) + b_1 \sum_{x\neq y} \left(1 - U^{1\times2}(x,y)\right) \right) \tag{3.17}$$

with $U^{i\times j}(x,y)$ the product of links along loop of the size $i \times j$, $\beta$ the coupling and $b_0 = 1 - 8b_1$ with $b_1 = -\frac{1}{2}$. The quark part of the action is Wilson twisted mass:

$$S_F[\chi,\overline{\chi}] = a^4 \sum_x \overline{\chi}(x) \left\{ \frac{1}{2} \left( \gamma_\mu \left( \bigtriangledown_\mu + \bigtriangledown_\mu^* \right) - a \bigtriangledown_\mu \bigtriangledown_\mu^* \right) + m_0 + i\mu_q\gamma_5\tau_3 \right\} \chi(x) \tag{3.18}$$

Here $\bigtriangledown_\mu$ and $\bigtriangledown_\mu^*$ are the covariant forward and backward derivatives, $\tau_3$ is the third Pauli matrix and $m_0$ and $\mu_q$ are the bare twisted and the untwisted quark masses. The quark field $\chi$ is the quark field in the twisted basis. For further details see [13, 14]. For $n_f = 2+1+1$ the action is

slightly more complicated (cf. [15]). The integral (3.16) cannot be calculated analytically. The Monte Carlo Method provides an unbiased estimate. Consider for clarity the more simple case

$$\langle O \rangle = \frac{1}{Z} \int \mathrm{D}\phi \exp[-S[\phi]] O(\phi) \tag{3.19}$$

The expectation value can be approximated by

$$\langle O \rangle \approx \frac{1}{K} \sum_{j=0}^{K} O(\phi_j) \tag{3.20}$$

To compute the sum a Markow chain of field configurations is generated, weighted by the factor $\exp[-S[\phi]]$. A more detailed presentation of Monte Carlo method can be found in [16].

Since the integral (3.15) involves only an integration over link variables, which takes a convenient form, one can solve it with the Monte Carlo method. Briefly, given a set of configurations, Wilson loops can be computed. From the VEV of the Wilson loop, one can determine the quark-antiquark potential.

In this work a set of 184 configurations is used, that has recently been generated on a $(32)^3 \times 64$-lattice for $n_f = 2 + 1 + 1$ dynamical quark flavours and coupling $\beta = 2.33$, hopping parameter $\kappa = 0.151064$ as well as quark masses $\mu = 0.0019$, $\mu_\sigma = 0.0577$ and $\mu_\delta = 0.0663$ (in units of the lattice spacing). Correlation functions for $\frac{r}{a} = 1, ..., 20$ and $\frac{\tau}{a} = 1, ..., 20$ were computed.

### 3.2.2. Smearing techniques

To compute the VEV of the Wilson loop one needs a quark-antiquark state with maximal overlap to the energy ground state referred to as $F(r)$ in equation (3.11). Otherwise the expression considered in equation (3.12) converges only for large $\tau$ to $V_{Q\overline{Q}}(r)$. To perform the average over neighbouring spacial loops of links yields a better overlap for the quark-antiquark state. This method is called **APE-smearing**[2].

The spacial resolution of a Wilson loop is highly focused, since the lines along the loop have a small spacial expense. A focused resolution in position space corresponds to a softened resolution in momentum space. In other words, a significant amount of momenta that contributes to the system's description in momentum space is very large. This increases the systems self-energy. Computing the quark-antiquark potential and the corresponding errors, one finds a bad signal to noise ratio. The hypercubic smearing **HYP2-smearing** solves this problem. Considering all temporal loops of links inside the hypercube of the width $a$ around the line of links to soften the resolution in position space yields a more focused resolution in momentum space. The self-energy decreases. To learn more details about smearing techniques see [17, 18].

## 3.3. The quark-antiquark potential: determination of the lattice spacing

It turned out that application of APE- and HYP2-smearing sets the potential and its error to an acceptable value.

Following the procedure described in the previous sections, the static quark-antiquark potential can be calculated. The potential is determined according to the following steps:

1. Calculation of $V_{\mathrm{eff}}(r, \tau)$ for $\frac{r}{a} = 1, ..., 20$ (cf. figure 3.2)
2. Fit of a (temporal) constant $V_{Q\overline{Q}}(r)$ to $V_{\mathrm{eff}}(r, \tau)$ in the fit range $\tau_{min} \leq \tau \leq \tau_{max}$ for each separation, cf. figure 3.2 and 3.3. The resulting function $V_{Q\overline{Q}}(r)$ is shown in figure 3.4.

[2]The term APE is based on Array Processor Experiment-machines, high performance computers used for QCD computations (cf. `http://hpc.desy.de/ape/`).

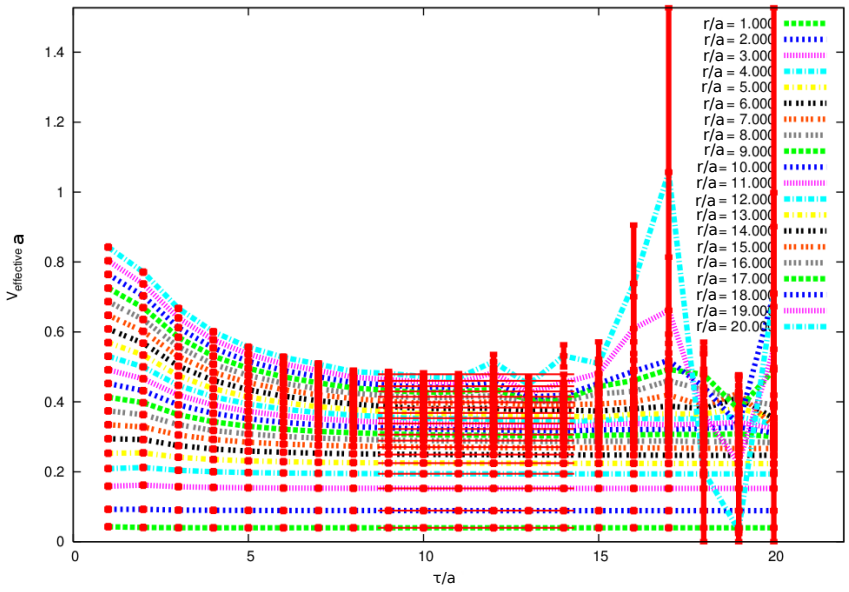


Figure 3.2.: Fit of a temporal constant

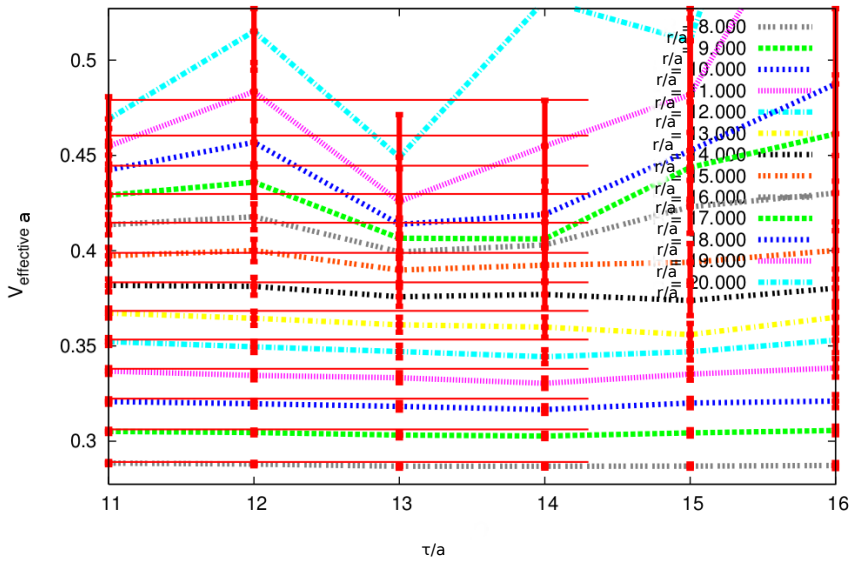


Figure 3.3.: Fit of a temporal constant in detail

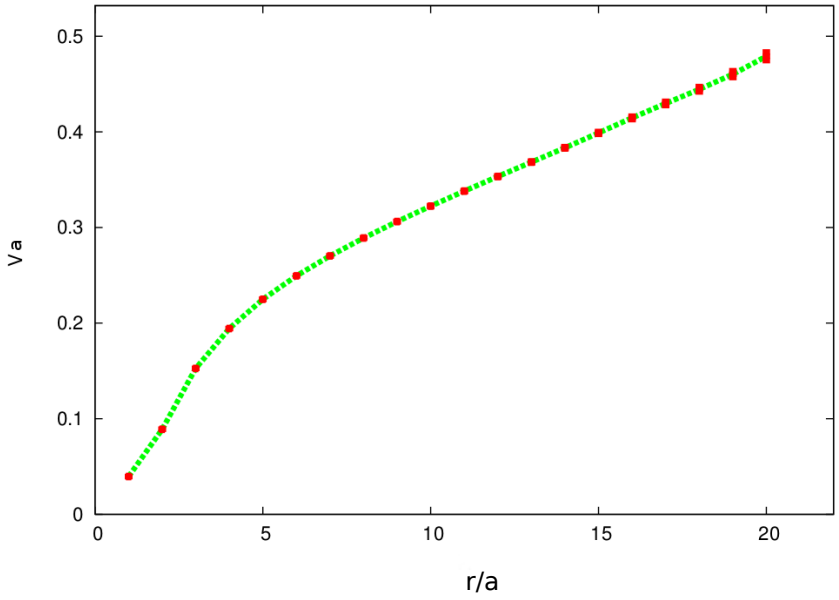


Figure 3.4.: $V_{Q\overline{Q}}(r)$

### 3.3.1. The Sommer parameter

The aim is to check, whether the lattice spacing for the configurations for $n_f = 2+1+1$ is in the same order of magnitude as the lattice spacing considered in the case of $n_f = 2$. The configurations were generated in order to deal with a similar lattice spacing. The Sommer parameter [19] is a quantity frequently used to set the scale for lattice calculations. Lattice results come in units of the lattice spacing $a$. To relate the lattice spacing $a$ to a physical unit one can compare the lattice result of an observable to the experimental result of the same observable.

A possible candidate is the quark-antiquark force $F_{Q\overline{Q}}(r) = \frac{\mathrm{d}}{\mathrm{d}r} V_{Q\overline{Q}}(r)$. The dimensionless quantity $F_{Q\overline{Q}} r^2$ can be crudely estimated from hadron experiments. The phenomenological value is

$$\frac{\mathrm{d}}{\mathrm{d}r} V_{Q\overline{Q}}(r)\Big|_{r=r_0} r_0^2 = 1.65 \qquad \text{with} \quad r_0 = 0.5\text{fm} \tag{3.21}$$

$r_0$ is the Sommer parameter.

### 3.3.2. Determination of the Sommer parameter

The lattice result $r_{0_{lattice}}$ for the Sommer parameter can be determined the following way: A function

$$V(r) = \boxtimes + \frac{\boxplus}{r} + \boxminus r \tag{3.22}$$

with fit parameters $\boxtimes$, $\boxplus$ and $\boxminus$ is fitted to $V_{Q\overline{Q}}(r)$. Since

$$\frac{\mathrm{d}}{\mathrm{d}r} V(r) = \boxminus - \frac{\boxplus}{r^2} \tag{3.23}$$

and

$$\frac{\mathrm{d}}{\mathrm{d}r} V_{Q\overline{Q}}(r)\Big|_{r=r_{0_{lattice}}} r_{0_{lattice}}^2 = 1.65 \tag{3.24}$$

which can be combined to

$$\left(\boxminus - \frac{\boxplus}{r^2}\right)\Bigg|_{r=r_{0_{lattice}}} r_{0_{lattice}}^2 = 1.65 \qquad \Leftrightarrow \qquad r_{0_{lattice}} = \sqrt{\frac{1.65 + \boxplus}{\boxminus}} \tag{3.25}$$

Now the fit to $V_{Q\overline{Q}}(r)$ is performed in a fit range $r_{min} \leq r \leq r_{max}$ (cf. figure 3.5).

The next step is to find the relation to the lattice spacing $a$.

In [20] one can find a result for the Sommer parameter for a lattice calculation with $n_f = 2+1+1$:

$$r_{0_{n_f=2+1+1}} = 0.4505\text{fm} \tag{3.26}$$

By comparison to the dimensionless fit result $r_{0_{lattice}}$ one finds $a$:

$$\frac{r_{0_{n_f=2+1+1}}}{r_{0_{lattice}}} = a \tag{3.27}$$

To check for systematic errors, $r_{0_{lattice}}$ is determined for several fit ranges in space and time. One range is kept fixed at a time (cf. tables 3.1 and 3.2).

Table 3.1.: spacial fit range fixed: $7a \leq r \leq 11a$

| $\tau_{min}..\tau_{max}$ in $a$ | $r_{0_{lattice}}$ | error |
|---|---|---|
| 10..15 | 10.499448 | 0.222224 |
| 9..14 | 10.294567 | 0.162429 |
| 8..13 | 10.060053 | 0.118867 |
| 10..13 | 10.445764 | 0.201179 |

Table 3.2.: temporal fit range fixed: $8a \leq \tau \leq 13a$

| $r_{min}..r_{max}$ in $a$ | $r_{0_{lattice}}$ | error |
|---|---|---|
| 7..11 | 10.060053 | 0.118867 |
| 6..10 | 10.092749 | 0.125759 |
| 8..12 | 10.033586 | 0.104405 |
| 9..13 | 10.037696 | 0.104646 |

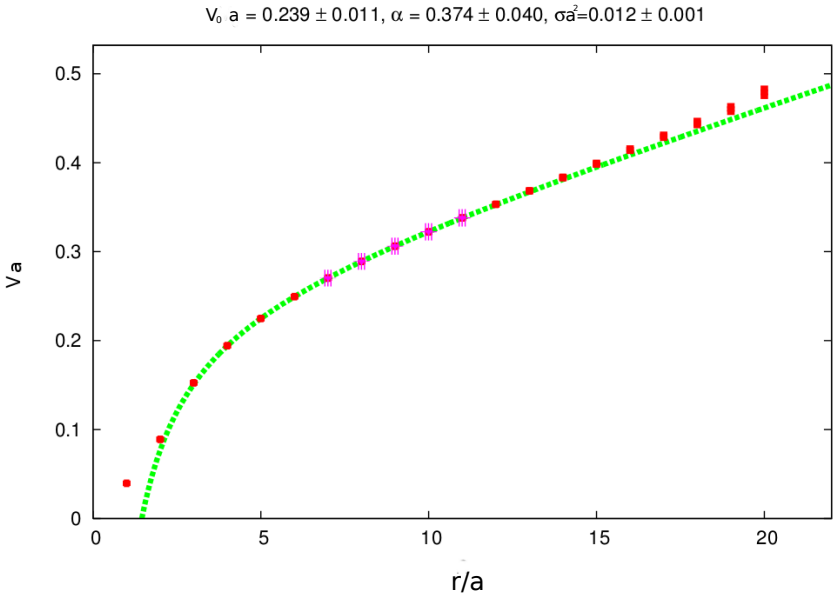


Figure 3.5.: Fit to determine $r_{0_{lattice}}$

Now the mean of all values for $r_{0_{lattice}}$ can be calculated. A (rather conservative) error is the square root of the quadratic sum of the individual errors.

One finds $\boxed{r_{0_{lattice}} = 10.19 \pm 0.43}$.

With (3.27) the lattice spacing is

$$a = \frac{r_{0_{n_f=2+1+1}}}{r_{0_{lattice}}} = \frac{0.4505}{10.19}\text{fm} = 0.0442\text{fm} \tag{3.28}$$

For $n_f = 2$ the finest lattice spacing is $a_{n_f=2} = 0.042$fm (cf. chapter 4).

The deviance from the just determined result is:

$$\frac{a - a_{n_f=2}}{a} = \frac{0.0442\text{fm} - 0.0420\text{fm}}{0.0420\text{fm}} \hat{=} 5.3\% \tag{3.29}$$

The lattice spacing for $n_f = 2 + 1 + 1$ and the finest available lattice spacing for $n_f = 2$ were expected to be similar. Both results differ by only 5%, so the lattice spacing determined from the data appears to be in a reasonable order of magnitude. However, the procedure described in this work has only the aim to give a first impression of the lattice spacing. For further investigations of the potential the choice of fit ranges in space and time might be improved, which might slightly change the determined results.

# 4. Preparation of lattice data

In the previous chapters methods to determine the quark-antiquark potential on the lattice, as well as in perturbation theory, were shown. The next step is to prepare the lattice data for the fitting procedure with perturbative formulae. Nonphysical lattice effects will be analysed and as far as possible removed.

## 4.1. Data modelling and Fourier transform

### 4.1.1. Modelling of lattice data at large distances

Starting point are four ensembles of gauge link configurations (cf. table 4.1) for $n_f = 2$ computed by the ETMC.

Table 4.1.: The four ensembles of gauge link configurations

| $\beta$ | $a$ in MeV | $(\frac{L}{a})^3 \times \frac{T}{a}$ | $m_{\mathrm{PS}}$ in MeV | number of gauges |
|---|---|---|---|---|
| 3.90 | 0.079(3) | $24^3 \times 48$ | 340(13) | 168 |
| 4.05 | 0.063(2) | $32^3 \times 64$ | 325(10) | 71 |
| | | | 449(14) | 100 |
| | | | 517(16) | 92 |
| 4.20 | 0.0514(8) | $48^3 \times 96$ | 284(5) | 46 |
| 4.35 | 0.0420(17) | $32^3 \times 64$ | 352(22) | 146 |

The quark-antiquark potential is computed analogous to the procedure presented in chapter 3 up to a quark-antiquark separation of $\frac{r}{a} = 10$. Calculations for large separations and especially off-axis separations are very time-consuming. For those reasons the lattice potential for $\frac{r}{a} > 10$ has to be computed by modelling to create a space-time volume that is large enough for further analysis. Because large distances correspond to small energies, the expectation is that details of the potential do not play a crucial rule for the corresponding part of the potential, so crude modelling is justified in this range. The first step to model data is to fit the formula, e.g.

$$V(r) = \boxtimes + \frac{\boxplus}{r} + \boxminus r \tag{4.1}$$

to the data by a $\chi^2$-minimizing fit in between a fit range $r_{min} \leq \ r \leq r_{max}$. The fit parameters are $\boxtimes$, $\boxplus$ and $\boxminus$. In the next sections other fit functions will be investigated. The values that correspond to $\frac{r}{a} > 10$ are calculated with the obtained fit formula. A scratch of the process is shown in figure 4.1.

Further details about the modelling process can be found in appendix B.

### 4.1.2. Discrete Fourier transform

The next step is to Fourier-transform the data to momentum space. To illustrate what happens in case of Fourier-transforming a quark-antiquark potential one can study a generic potential. In the beginning the continuous potential

$$V(r) = V_0 - \frac{\pi}{12r} + \sigma r \quad \text{with} \quad r = \sqrt{x^2 + y^2 + z^2} \tag{4.2}$$

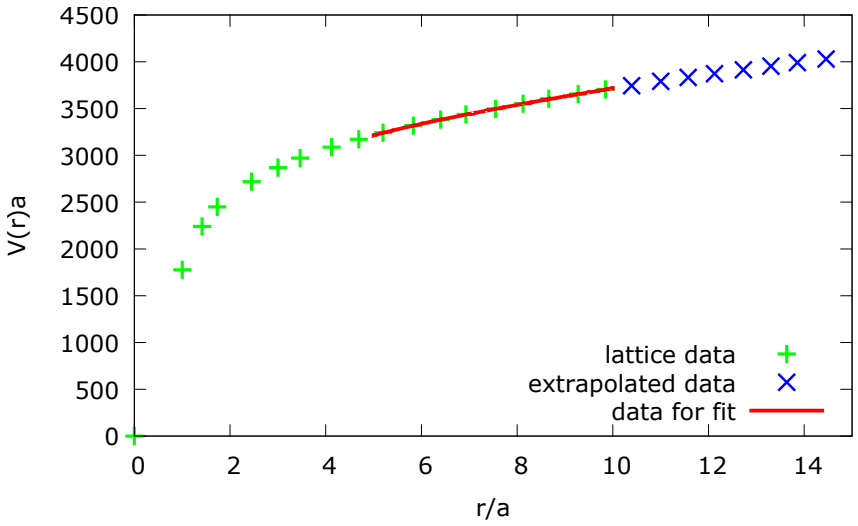


Figure 4.1.: Extrapolation of lattice data

is considered. The string tension $\sigma$ is given by the Sommer scale $r_0$ by the relation

$$1.65 = |F(r_0)|{r_0}^2 = \left|\frac{d}{dr}V(r_0)\right|{r_0}^2 \quad \text{with}\, r_0 = 0.5\text{fm} \Rightarrow \quad \sigma = \sigma(r_0) = 5.55\frac{1}{\text{fm}^2} \tag{4.3}$$

Next the potential $V(r)$ is discretized (cf. figure 4.2). With the lattice spacing $a$ one finds for the position vector $\vec{r}$:

$$\vec{r} \to a\vec{n} = a\begin{pmatrix} n_x \\ n_y \\ n_z \end{pmatrix}. \tag{4.4}$$

To get a dimensionless quantity, multiply with $a$:

$$V(\vec{r}) \to \hat{V}(r) = V(n)a = V_0 a - \frac{\pi}{12n} + \sigma a^2 n \quad \text{with} \quad n = |\vec{n}|, \quad \vec{n} \in \mathbb{N}^3 \tag{4.5}$$

Although the potential is spherically symmetric it has to be considered as a three-dimensional quantity. The DFT works in three dimensions. The potential values are stored in a three-dimensional array. To underline this the potential will be referred to as $V(\vec{n})$. Implementing the periodic boundary conditions, in detail the potential receives the following shape:

$$V(\vec{n}) = V(n_x, n_y, n_z) = \begin{cases} V(n_x, n_y, n_z) & \text{if} \quad n_x \le N/2, \quad n_y \le N/2, \quad n_z \le N/2 \\ V(N-n_x, n_y, n_z) & \text{if} \quad n_x > N/2, \quad n_y \le N/2, \quad n_z \le N/2 \\ V(n_x, N-n_y, n_z) & \text{if} \quad n_x \le N/2, \quad n_y > N/2, \quad n_z \le N/2 \\ V(n_x, n_y, N-n_z) & \text{if} \quad n_x \le N/2, \quad n_y \le N/2, \quad n_z > N/2 \\ V(N-n_x, N-n_y, n_z) & \text{if} \quad n_x > N/2, \quad n_y > N/2, \quad n_z \le N/2 \\ V(N-n_x, n_y, N-n_z) & \text{if} \quad n_x > N/2, \quad n_y \le N/2, \quad n_z > N/2 \\ V(n_x, N-n_y, N-n_z) & \text{if} \quad n_x \le N/2, \quad n_y > N/2, \quad n_z > N/2 \\ V(N-n_x, N-n_y, N-n_z) & \text{if} \quad n_x > N/2, \quad n_y > N/2, \quad n_z > N/2 \end{cases} \tag{4.6}$$

The next step is to analyse the potential in momentum space. Therefore the discrete Fourier transform (DFT) in three dimensions is applied. The DFT is:

$$\hat{V}(\vec{n}) \to \hat{\tilde{V}}(\vec{k}) = \frac{a}{\sqrt{N^3}} \sum_{n_x,n_y,n_z=0}^{N-1} V(\vec{n}) \mathrm{e}^{\frac{2\pi i \vec{k}\cdot\vec{n}}{N}} \tag{4.7}$$

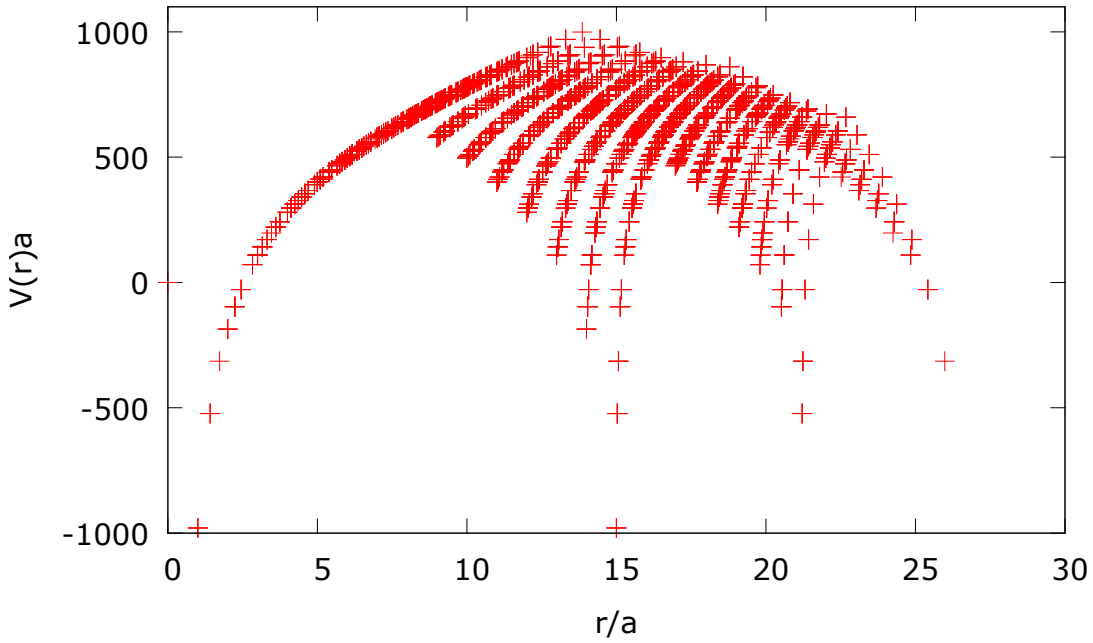


Figure 4.2.: Generic potential in position space for $\frac{L}{a} = 16$

Looking at the continuum limit one finds the proportionality factor that is necessary to be able to compare lattice to continuum results:

$$\begin{aligned}\hat{\tilde{V}}(k) &\overset{\vec{p}=\frac{2\pi\vec{k}}{Na}}{\longrightarrow} \lim_{a\to 0} \frac{a}{\sqrt{N}^3}\frac{1}{a^3} \sum_{n_x,n_y,n_z=0}^{N-1} a^3 V(p) \mathrm{e}^{\frac{2\pi i\vec{k}\cdot\vec{n}a}{Na}} \\ &= \frac{a}{(\sqrt{N}a)^3}\int \mathrm{d}^3 r V(r)\mathrm{e}^{i\vec{r}\cdot\vec{p}} \\ &= \frac{1}{a^2}\frac{1}{\sqrt{N}^3}\int \mathrm{d}^3 r V(r)\mathrm{e}^{i\vec{r}\cdot\vec{p}} \\ &\equiv \tilde{V}(p) \end{aligned} \tag{4.8}$$

The steps shown in this section are applied to the lattice data accordingly. In the following, momentum space results will be stated in physical dimensions MeV (for the momentum) and $\mathrm{MeV}^{-2}$ (for the potential). The plots in this work will show an energy range of at most [0MeV..25000MeV] since the energy range beyond definitely does not yield reliable data for $p > p_{max} = \frac{\pi}{a} \simeq 15000\mathrm{MeV}$ anyway.

### 4.1.3. The quark-antiquark potential for $r = 0$

For $r = 0$ no lattice data is available since at a quark-antiquark separation of 0 the potential is physically not meaningful. A lattice computation only makes sense for lattice separations that are large in comparison to the lattice spacing, otherwise the discretization effects take vast proportions. Nevertheless this value is important to provide the full potential. The value of $V(r)$ for $r = 0$ can be chosen arbitrary. For the Fourier transform the choice of this value does not play a crucial role. The following calculation shows this (for simplicity a continuous Fourier transform is considered):

$$\begin{aligned}\tilde{V}(k) &= \int \mathrm{d}r(V_0\delta(r) + V(r))\mathrm{e}^{ikr} \\ &= V_0 \int \mathrm{d}r\delta(r)\mathrm{e}^{ikr} + \int \mathrm{d}rV(r)\mathrm{e}^{ikr} \\ &= V_0\mathrm{e}^{ik0} + \int \mathrm{d}rV(r)\mathrm{e}^{ikr} \\ &= V_0 + \int \mathrm{d}rV(r)\mathrm{e}^{ikr} \end{aligned} \tag{4.9}$$

$V_0$ is an additional constant. For the fitting procedure in momentum space the choice of the additional constant in position space is irrelevant. One can choose $V_0 = 0$.

### 4.1.4. Selecting momenta

In order to reduce nonphysical errors, a method of selecting data is applied [21] to the potential in momentum space: The so called Cylinder Cut chooses potentials of momenta with at most a finite number of momentum units of distance from the lattice diagonal $\left(\tilde{V}(p_x, p_y, p_z), \quad p_x = p_y = p_z\right)$. Experience shows that thereby lattice spacing errors carry less weight. The Cylinder Cut yields a more distinct curve (cf. figure 4.3) which is beneficial for the fitting procedure. The cylinder cut is applied to each data set considered in this work.

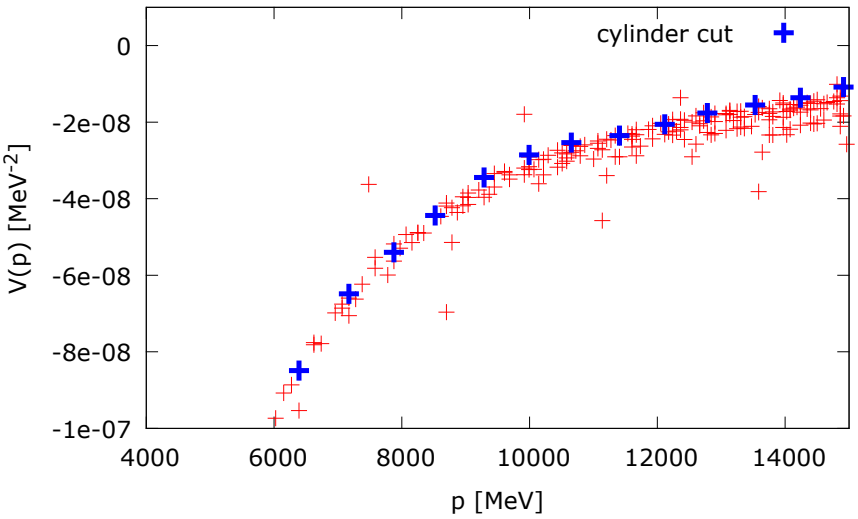


Figure 4.3.: Selection of momenta (Cylinder Cut)

## 4.2. Lattice effects

To check for systematic errors due to finite lattice spacing and extent of the data set in momentum space it is advisable to study the effects that depend on those parameters.

Before starting with advanced considerations some basic facts shall be contemplated. There are two ways to get a physical result from a lattice calculation. Both approaches should describe the same physics. Consider the 1d-case. $N_L$ is the spacial lattice extent and $a$ the lattice spacing:

1. The volume $N_L a$ grows to infinity ($N_L \to \infty$) for fixed $a$.

2. The volume becomes continuous ($N_L a = \text{const}$, $N_L \to \infty$, $a \to 0$).

In position space the separation on the lattice is

$$n = \frac{r}{a} \quad \text{with} \quad n \in [0, .., N_L - 1] \tag{4.10}$$

In case 1 the volume grows, i.e. $N_L a$ grows with growing $N_L$. In case 2 the volume is constant, i.e. $N_L a$ does not change with growing $N_L$.

In momentum space it is the other way round. On the lattice the momentum $p$ takes the values:

$$p \in \left[ -\frac{\pi N_L}{a N_L}, .., \frac{\pi (N_L - 1)}{a N_L} \right] \tag{4.11}$$

In case 1 the volume grows, the values of $p$ do not change with increasing $N_L$. In case 2 the volume is constant, the values of $p$ grow with increasing $N_L$.

Those relations are important for labelling and scaling the axes correctly.

### 4.2.1. The infinite volume limit

How far the data is extrapolated does not play in important rule for the shape of the potential for large momenta as the following analysis shows: The lattice spacing $a$ is kept constant ($a = 0.042\text{fm}$) for one of the given lattice ensembles (cf. table 4.1) and $N_L$ is varied, $V_0 = \tilde{V}_0 = 0$. The more $N_L$ grows, the bigger the volume gets. In the plot the considered momentum range is the same for each $N_L$ (cf. figure 4.4).

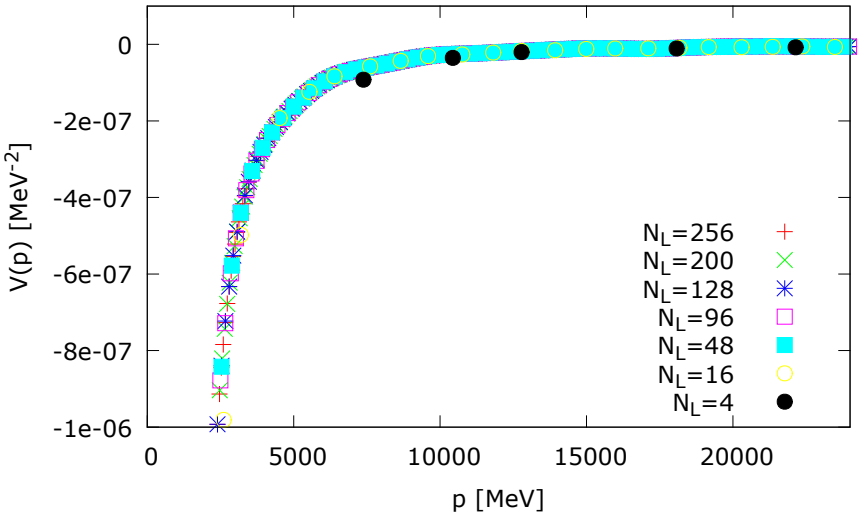


Figure 4.4.: Comparison of lattice and continuum potential (increasing volume)

Note that for $N_L = 4$ there is no extrapolation necessary, so all points are lattice data points[1].

### 4.2.2. Continuum limit

To study the following effect the discretized version of the generic potential (4.7) is used. To check the absence of discretization effects the volume $aN_L$ is kept constant, but $a$ and $N_L$ are varied (cf. figure 4.5).

[1] During the extrapolation process no replacement by generic values takes place, cf. listing B.2 in appendix B for further details.

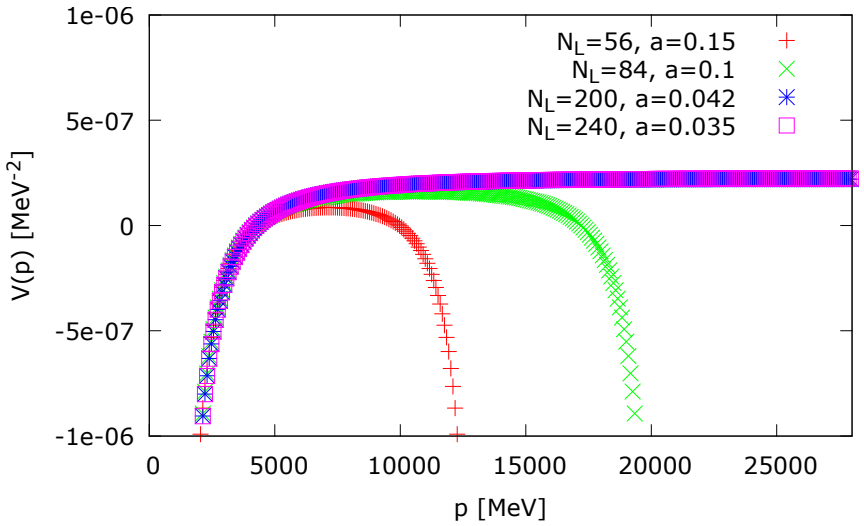


Figure 4.5.: Comparison of lattice and continuum potential (constant volume)

One can see in figures 4.4 and 4.5 that for a large lattice extent ($N_L \gtrsim 200$) and a small lattice spacing neither finite volume nor discretization effects play a crucial role in a momentum range up to $\backsimeq$ 5000MeV. This observation will be important for the choice of fit range and lattice extent for a fit to perturbative expressions (cf. chapter 5).

## 4.3. Analysis of artefacts that manifest in momentum space due to modelling of the potential

Extrapolating lattice values to bigger distances means getting a point of transition between physical and generic values. At this point, discontinuities like gaps and kinks can appear which show up clearly after a Fourier transform[2], especially when looking at the derivative of the momentum space potential (cf. equation 2.1) on the diagonal. This quantity can be understood as a sort of tree-level coupling. It is referred to as $\alpha(p)$:

$$\frac{3\overline{p}^3}{32\pi}\frac{V(p_{i+1})-V(p_i)}{p_{i+1}-p_i}=\alpha(p), \qquad \overline{p}=\frac{p_i+p_{i+1}}{2} \tag{4.12}$$

Looking at $\alpha(p)$, one finds a rather curly than monotonous behaviour.

[2] due to the Gibbs phenomenon [22]

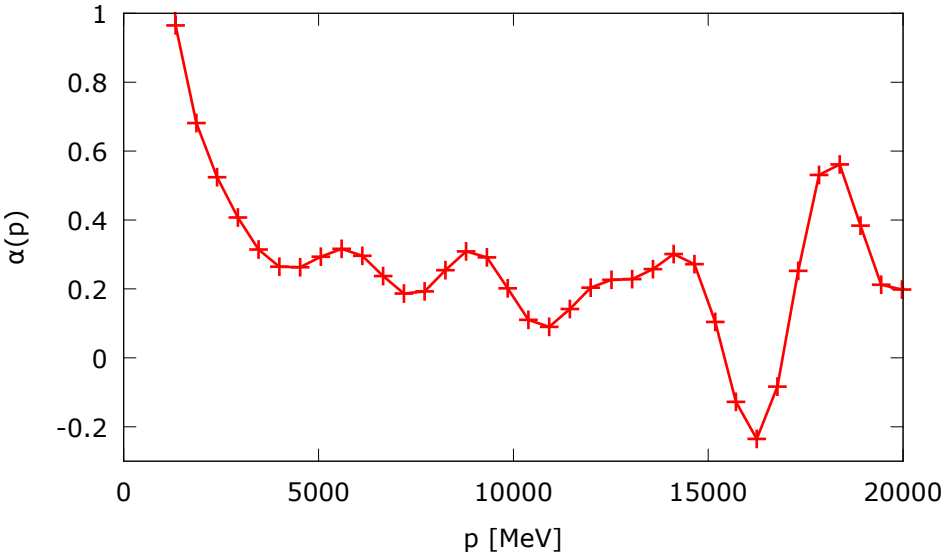


Figure 4.6.: The tree-level coupling $\alpha(p)$ on the lattice

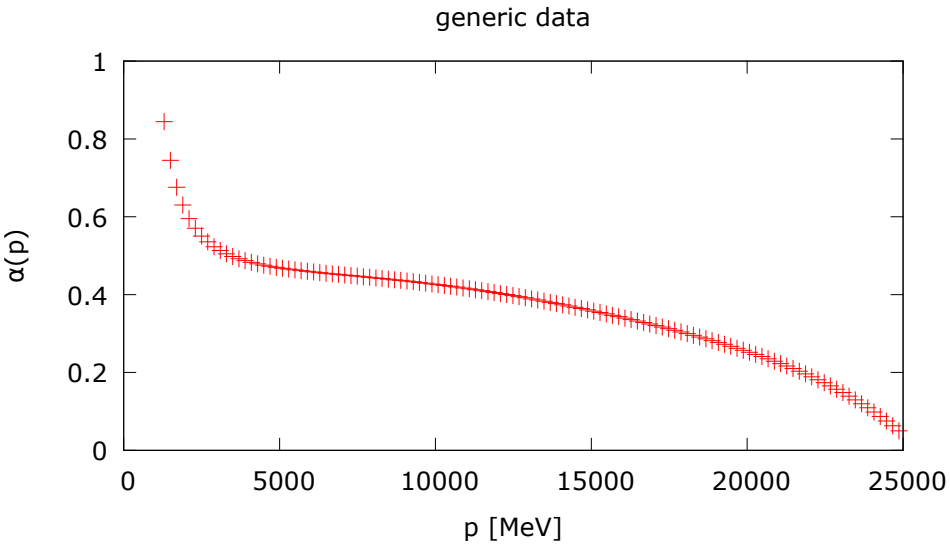


Figure 4.7.: $\alpha(p)$ from a derivative of generic data

One might suspect that the curls do not depend of the periodic boundary conditions of the potential. One can observe no curls in the case of a generic potential without extrapolated data. In figure 4.7 $\alpha(p)$ for generic data is shown. The generic data has been created in the following way: the potential (4.2) has been fitted to lattice data. Using the resulting fit parameters, a generic data set has been created. $\alpha$ has been derived by application of (4.12).

Another observation is that the curls seem to be influenced by the variation of the range at which the lattice values are fitted for modelling. The smaller the distance between upper boundary of this fit range and the point of transition to modelled data at $\frac{r}{a} = 10$ is, the smaller the curls' amplitude gets. To show this two different approaches to determine $\alpha(p)$ are presented:

1. derivation of $\alpha$ from a direct fit on the potential in momentum space (2.1) in leading order on the basis of several fit windows of a width of 600MeV (label A)

2. derivation of $\alpha$ from (4.12) (label B)

The fit ranges for the data modelling in position space are varied in both cases. For approach A on the horizontal axis the lower boundary of the fit window in momentum space $p_l$ and upper boundary of the fit range in momentum space $p_l + 600\text{MeV}$ for each window $l$ are plotted. On the vertical axis the corresponding fit value is plotted. This yields a step-shaped graph. The results can be found in figure 4.8. The graph is labelled with the fit ranges in position space as well as with 'A' or 'B' according to the approach. Both approaches yield towards the same trend: The closer the upper boundary of the fit range in position space to $\frac{r}{a} = 10$ the smaller the amplitude of the curls. From this it follows that it is advisable to choose a fit range with the upper boundary $r_{max} = 10a$.

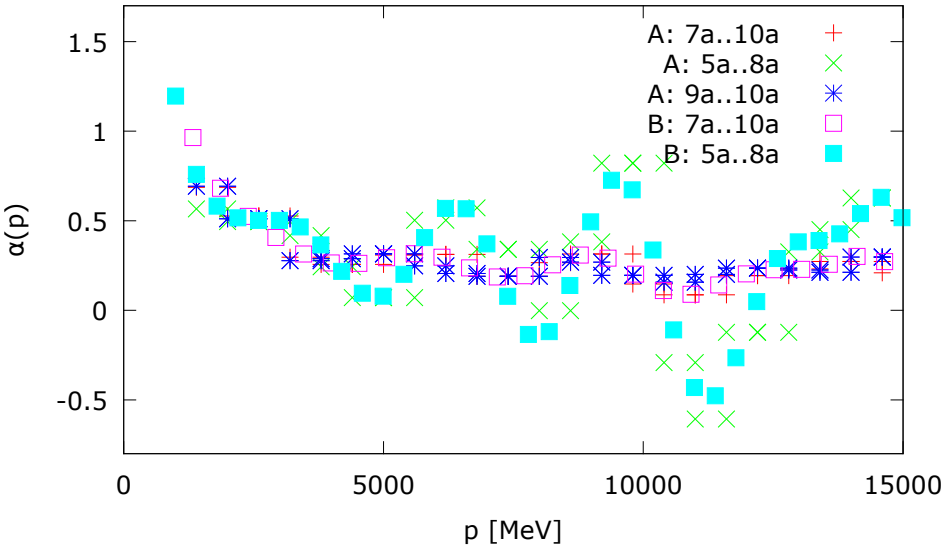


Figure 4.8.: $\alpha(p)$ from a derivative and directly fitted

### 4.3.1. The source of the curls

To receive a better understanding of the curly behaviour of $\alpha(p)$, in the following the situation is reproduced on the basis of toy models. The curls apparently seem to depend on the position and width of a discontinuity in the potential due to the data modelling in position space. Using the toy model (2.1) one can investigate how a gap or a kink influences the amplitude and wavelength of the curls of $\alpha(p)$.

Provoking a gap in the position space potential at $\frac{r}{a} = 10$ by adding a constant for $\frac{r}{a} > 10$ (cf. figure 4.9) causes a wavy behaviour of the momentum space potential (cf. figure 4.10) and the $\alpha$ plot (figure 4.11) looks very much alike figure 4.6. If the gap has the width of $0.005a$, the curls are in the same order of magnitude as in the case of lattice data. This gap is too small to be visible to the naked eye - if one looks at the position space potential, no gap can be identified (cf. 4.12).

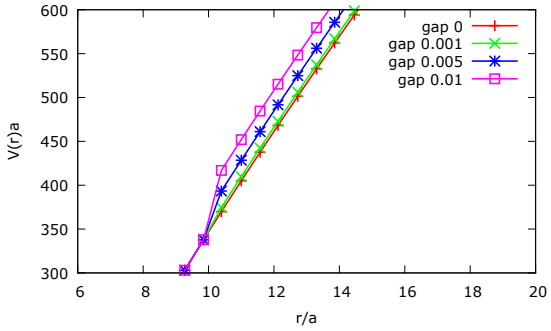


Figure 4.9.: Gap in position space

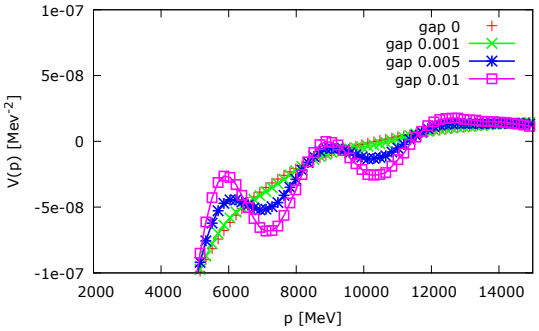


Figure 4.10.: Momentum space

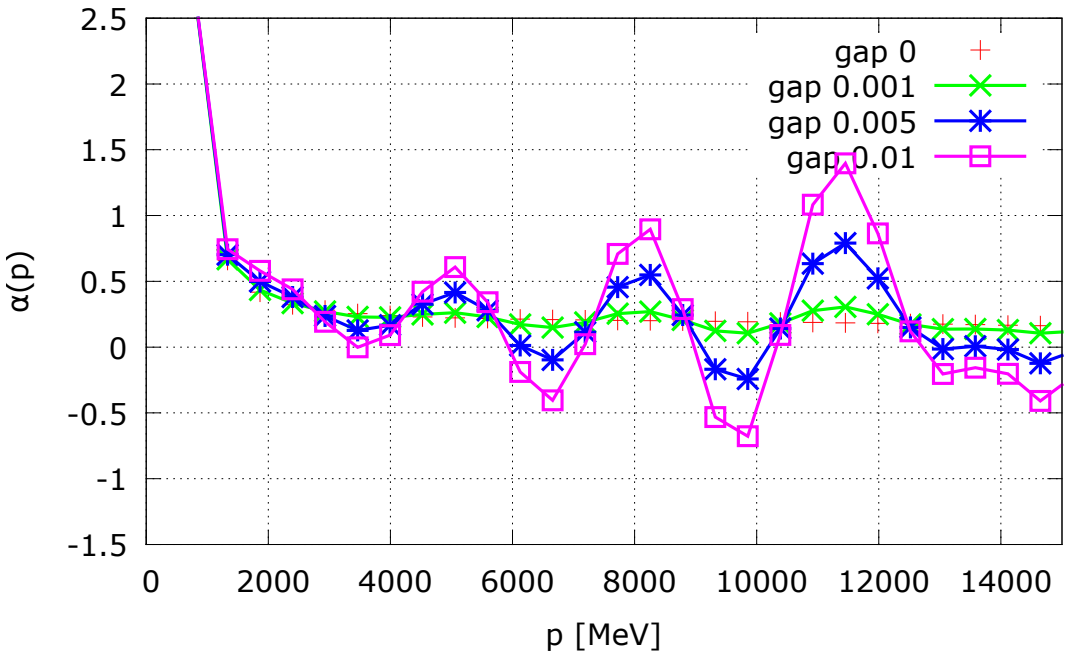


Figure 4.11.: $\alpha$ (toy-model: gap)

Provoking a kink by variation of the $\sim \frac{1}{r}$-part of the potential one finds a similar behaviour. The curves in figure 4.13, 4.14 and 4.15 are labelled with the relative factor

$$\kappa = \left. \frac{\frac{\mathrm{d}}{\mathrm{d}r} V_{in}(r)}{\frac{\mathrm{d}}{\mathrm{d}r} V_{out}(r)} \right|_{r=10a} \tag{4.13}$$

which measures the ratio of the gradients of the "inner" ($\frac{r}{a} \leq 10.0$) and the "outer" ($\frac{r}{a} > 10.0$) part of the potential at the $\frac{r}{a} = 10$. The curls of $\alpha(p)$ are in the same order of magnitude as in the lattice data case, if $\kappa = 1.12$, which means that the gradients of the "outer" and the "inner" part of the potential differ by 12% at the transition point (cf. figure 4.15).

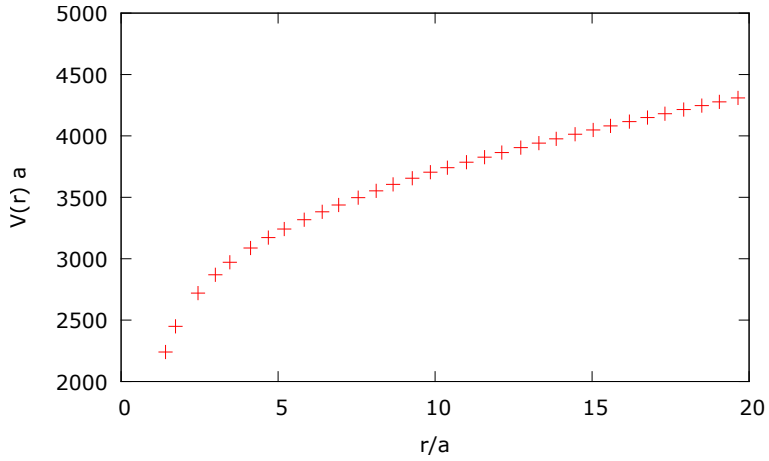


Figure 4.12.: Potential in position space: no discontinuities can be seen with the naked eye

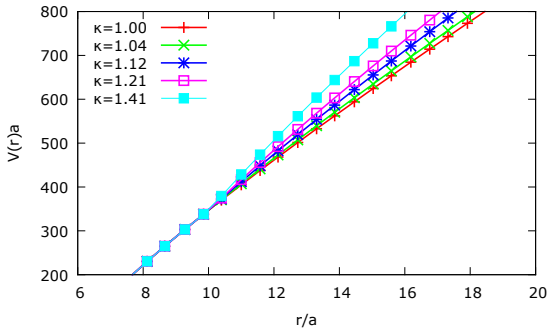


Figure 4.13.: Kink in position space

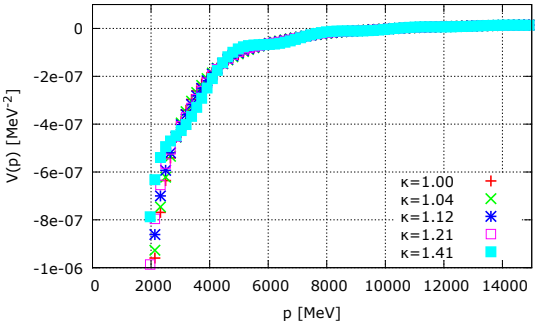


Figure 4.14.: Momentum space

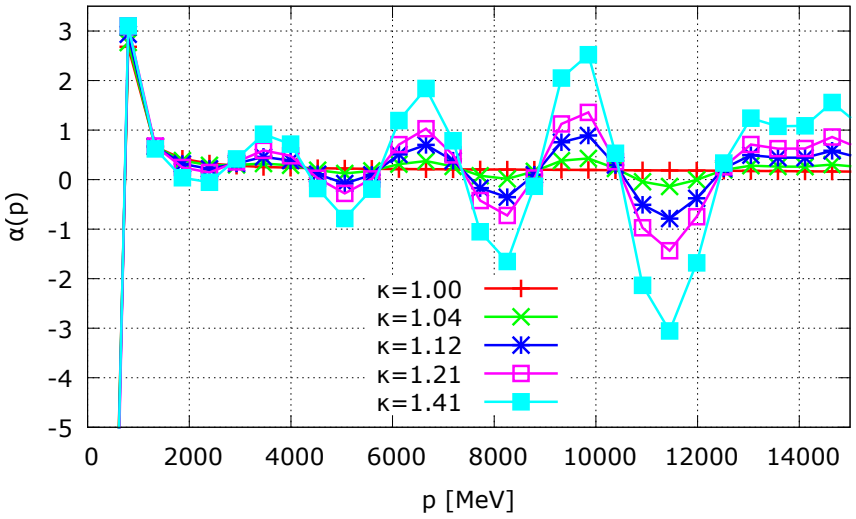


Figure 4.15.: $\alpha$ (toy-model: kink)

One can collect further evidence about the brink or gap to be the cause of the curls measuring

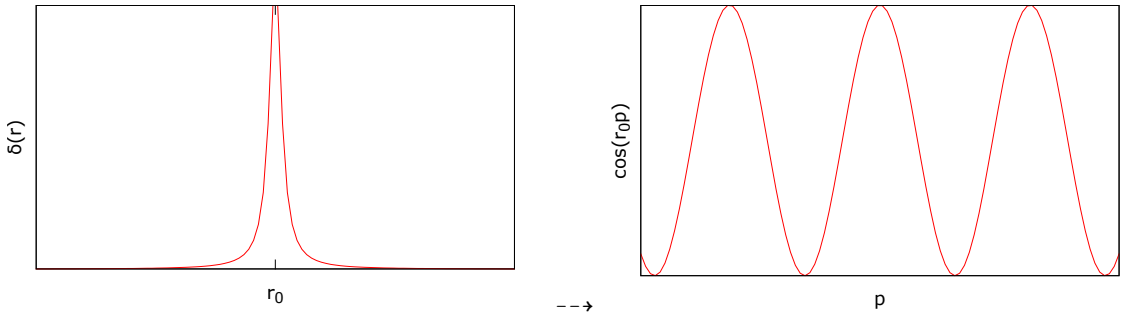


(a) A location in position space... (b) ...corresponds to a wave in momentum space.

Figure 4.16.

the wavelength of the curls in MeV in momentum space. So one can detect the location of the gap respectively the kink. A position $r_0$ described by $\delta(r-r_0)$ in position space is a Fourier-transformed (FT) cosine wave in momentum space (cf. figure 4.16 ):

$$\delta(r-r_0) = \frac{1}{2\pi}\int \mathrm{d}p\, \mathrm{e}^{ipr}\, \mathrm{e}^{-ipr_0} = \mathrm{FT}\left(\mathrm{e}^{-ipr_0}\right) = \mathrm{FT}\left(\cos(r_0 p) + i\sin(r_0 p)\right) \tag{4.14}$$

Consider only the real part. The wavelength is about $\lambda_p = 3000\mathrm{MeV}$. One finds[3]:

$$\cos\left(r_0 p\right) = \cos\left(\frac{2\pi}{\lambda_p}p\right) = \cos\left(\frac{2\pi}{1800\mathrm{MeV}}p\right) \overset{1=197\mathrm{MeV\ fm}}{=} \cos\left(\frac{2\pi 197\mathrm{fm}}{1800}p\right) \Rightarrow x_0 p = \frac{197\mathrm{fm}}{1800}p \tag{4.15}$$

Solving for $r_0$ yields: $r_0 = 0.413\mathrm{fm} = \frac{r_0}{a}a = \frac{0.066}{0.042}a = 9.82a$. The expected discontinuity are located at $10a$, so the estimated value is in the right order of magnitude.

### 4.3.2. Gaussian blur

In order to study the discontinuity in the potential due to the data modelling in position space further, one can try to smooth the point of transition by applying a Gaussian blur to the modelled data. Since the toy-model analysis in the previous section showed that discontinuities cause the curly behaviour of $\alpha(p)$, it is expected to fade, if gaps and kinks in the potential are removed. To apply a Gaussian blur means to weight neighboured points in a clever way (so-called masking). The blur weights the points according to a Gaussian distribution with the width $\sigma_{\mathrm{Gauss}}$. The process is iterated several times. The figures 4.17, 4.18 and 4.19 show the results in position and momentum space as well as the behaviour of $\alpha(p)$.

One can see that the graphs look smooth in position space as well as in momentum pace. This is also the case if no blur is applied, so the blur does not cause strong distortions of the potential. Furthermore the amplitude of $\alpha(p)$ even grows as the number of iterations increase for each value of $\sigma_{\mathrm{Gauss}}$. The blur does not show the desired effect at all. Against the expectation the blur cannot improve the behaviour of $\alpha(p)$. The reasons for this are currently not understood.

### 4.3.3. Adaptation of the fitting procedure to make the curls vanish

One idea to make the curls vanish is to adapt the fit function for the data modelling in position space. The fit function shall provide a smooth transition between lattice data and modelled data. For example, one can improve the transition by performing a one-parameter fit with the constraint,

[3] conversion of MeV to fm in natural units, cf. e.g. [23]

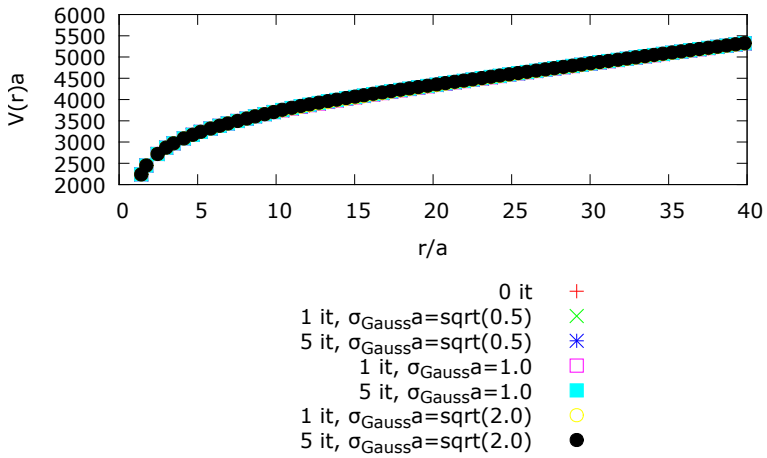


Figure 4.17.: Gaussan blur - position space

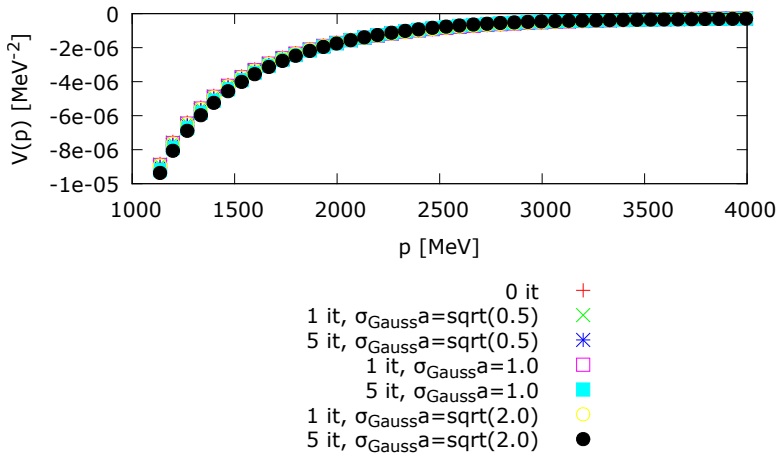


Figure 4.18.: Gaussan blur - momentum space

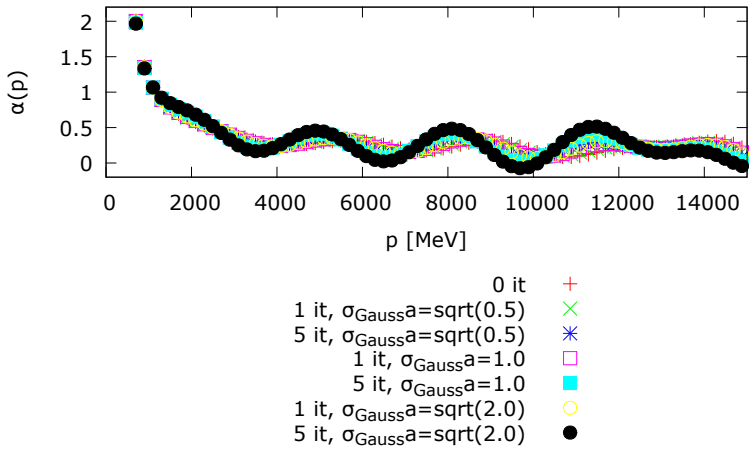


Figure 4.19.: Gaussan blur - behaviour of $\alpha$

that the fitted graph intersects the lattice point with the greatest distance. The fit model is:

$$V(r) = \tilde{V} + \alpha\left(\frac{1}{r} - \frac{1}{\tilde{r}}\right) + \sigma_{fix}(r - \tilde{r}) \tag{4.16}$$

with $\sigma_{fix} = 5.55\frac{1}{\text{fm}^2}a^2$ and $\tilde{r}$ and $\tilde{V}$ the largest available lattice distance and associated potential value.

Another way to smooth the transition point between lattice data and modelled data is to vary the number of fit parameters further. The following fit models have been investigated:

- 1 parameter: $V_1(r) = \tilde{V} + \boxtimes\left(\frac{1}{r} - \frac{1}{\tilde{r}}\right) + \sigma_{fix}(r - \tilde{r})$
- 2 parameters: $V_2(r) = \boxminus - \frac{\boxtimes}{r} + \sigma_{fix}r$
- 3 parameters: $V_3(r) = \boxminus - \frac{\boxtimes}{r} + \boxplus r$
- 4 parameters: $V_4(r) = \boxminus - \frac{\boxtimes}{r} + \boxplus r + \frac{\oslash}{r^2}$
- 4 parameters: $V_4^*(r) = \boxminus - \frac{\alpha_{fix}}{r} + \sigma_{fix}r + \frac{\oslash}{r^2} + \frac{\odot}{r^3} + \frac{\bigcirc}{r^4}$
- 5 parameters: $V_5(r) = \boxminus - \frac{\boxtimes}{r} + \boxplus r + \frac{\oslash}{r^2} + \frac{\odot}{r^3}$

With $\alpha_{fix} = \frac{\pi}{12}$ a phenomenological value (cf. the generic model 4.2). Symbols like $\boxminus$ and $\boxtimes$ stand for the fitting parameters. The fit ranges are as follows:

- 1 and 2 parameters: $8 \leq \frac{r}{a} \leq 10$
- 3 parameters: $6 \leq \frac{r}{a} \leq 10$
- 4 parameters: $4 \leq \frac{r}{a} \leq 10$
- 5 parameters: $3 \leq \frac{r}{a} \leq 10$

The fit ranges were chosen in the manner that the reduced $\chi^2$-value was small enough:

$$\frac{\chi^2}{\text{dof}^4} \leq 1 \tag{4.17}$$

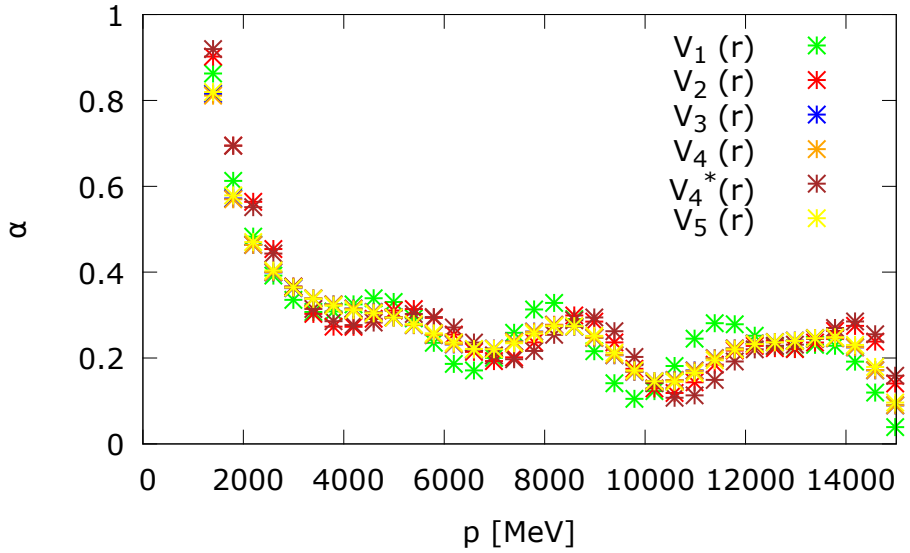


Figure 4.20.: $\alpha$ depending on the fit model

One can see the influence on $\alpha$ in figure 4.20.

The Fourier transform seems to be very sensitive to a discrepancy of the mathematical nature of the lattice values and the modelling function. Only a many-parameter fit can very slightly improve the behaviour of the curve. Generally there is no physical constraint for the choice of the model. So there is no reason to prefer one of them. One can suspect that a many-parameter fit can model the mathematical shape of the lattice data better. Anyway an increasing number of parameters cannot improve the behaviour of $\alpha(p)$ satisfactorily.

In summary, the findings of the previous sections show that the curly behaviour of the tree level coupling $\alpha(p)$ is due to discontinuities in the potential that occur because of the data modelling for large distances. However, the application of a Gaussian blur does not show the desired effect of smoothing the potential. Also a variation of the data model cannot solve the problem. The phenomenon of the curls of $\alpha(p)$ is not fully understood yet. The curls cannot be completely removed.

Nevertheless the perturbative formulae are fitted to the potential in momentum space and not to its tree-level derivative. The wiggly behaviour is less significant to the potential itself.

## 4.4. Transition point

In the analysis in the following chapter, the point of transition between lattice and modelled data will be at $\frac{r}{a} = 10$ to include as many physical results as possible. Nevertheless it is important to check that a shift of the transition point to smaller distances has no crucial effect on the data. For the check the 4-parameter fit model $V_4{}^*(r)$ is used. The fit range is $7 \leq \frac{r}{a} \leq 10$. Shifting the point of transition to $\frac{r}{a} = 8$ or $\frac{r}{a} = 7$ means to use modelled data points for $\frac{r}{a} > 8$ respectively $\frac{r}{a} > 7$. The shift of the transition point might have effects on the curly behaviour of the tree-level coupling $\alpha(p)$. This should be analysed in the future. Nevertheless, figures 4.21, 4.22 and 4.23 show that the data does not change significantly as the transition point is shifted.

[4] degrees of freedom: number of values in fit range minus number of fit parameters

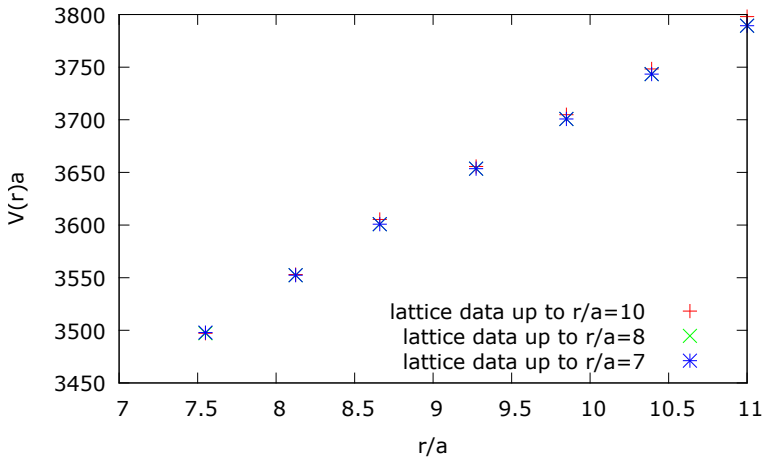


Figure 4.21.: Shift of transition point - position space

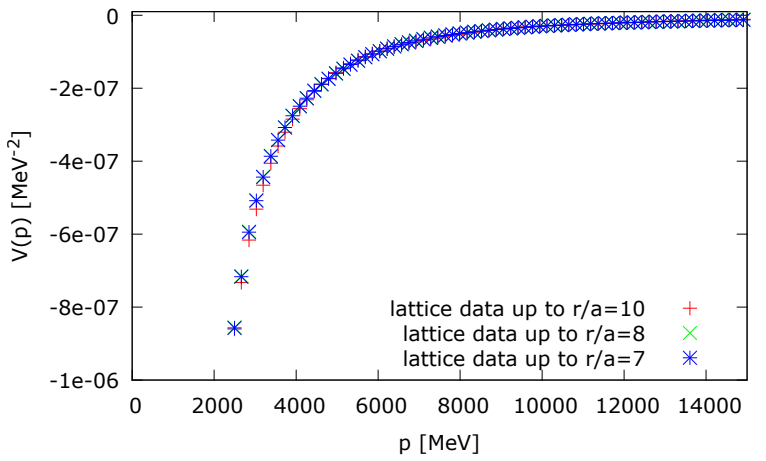


Figure 4.22.: Shift of transition point - momentum space

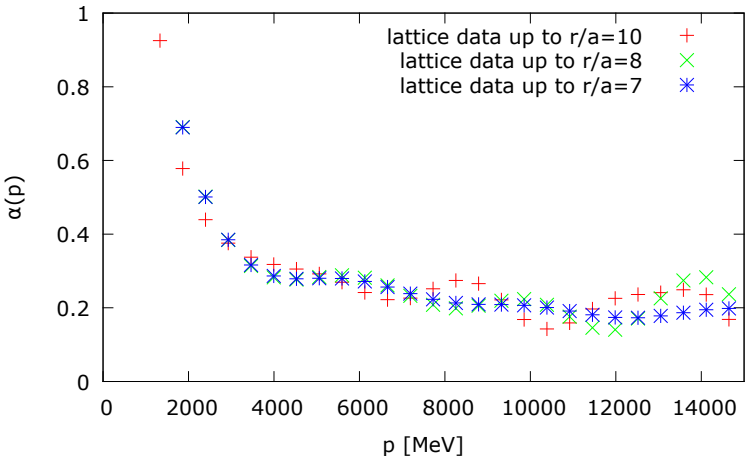


Figure 4.23.: Shift of transition point - effects on $\alpha$

## 4.5. Symanzik improvement

For big momenta respectively small distances the Coulomb part of the physical potential dominates. One can calculate the tree-level potential on a lattice using a special recursive method up to arbitrary precision and compare it to the corresponding tree-level calculation in continuum.

The comparison shows how to shift the potential to annihilate discretization errors.

The shifts along the $p$-axis are afterwards applied to the momentum values of the extrapolated lattice data. In figure 4.24 one can see the effect on the lattice data.

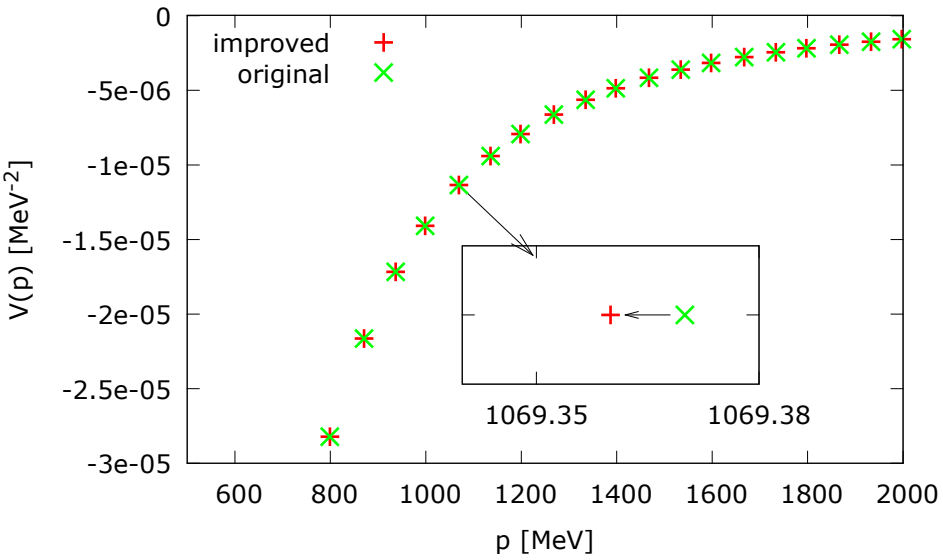


Figure 4.24.: original data vs. improved data

This procedure is called Symanzik improvement. It is applied to all data analysed in this work. In momentum space the effect is smaller than in position space (cf. [3]), nevertheless it is a conceptual improvement. Details about the procedure can be found in appendix C.

# 5. Fitting procedure

In this chapter $\Lambda_{\overline{MS}}$ is determined by fitting perturbative formulae for the static quark-antiquark potential in momentum space (cf. chapter 2) to the corresponding lattice results (cf. chapter 4).

## 5.1. The Jackknife error

To determine a proper error for lattice results the Jackknife method [24] can be applied. The procedure is the following: Consider a list of $N$ measurements for a data set of $J$ entries $x_i(1), x_i(2), ..., x_i(J)$ with $1 \leq i \leq N$. Let $\overline{n}_j$ be the means of the full list.

1. The first measurement is thrown out.
2. A reduced set of $N-1$ values is left behind.
3. Do a statistical analysis to the reduced sample, name the result $n_{j1}$
4. Throw out the second measurement.
5. Do a statistical analysis to the reduced sample of $N-1$ measurements, name it $n_{j2}$
6. Repeat until a set of $N$ $(n_{j1}, n_{j2}, ...n_{jN})$ values is generated

Based on this list compute the Jackknife error $\sigma$:

$$\sigma_j = \sqrt{(N-1)\sum_{i=1}^{N} \frac{(n_{ji} - \overline{n}_j)^2}{N}} \tag{5.1}$$

The lattice data analysed in this work consists of a full set of lattice values for the static potential as well as several reduced sets.

## 5.2. Variation of perturbative formulae and input parameters to the fitting procedure

### 5.2.1. Fitting procedure for extrapolation in position space

In section 4.3.3 several models for the fit during the extrapolation procedure are introduced. In the following three of them will be used in order to determine $\Lambda_{\overline{MS}}$:

- 2 parameters: $V(r) = \boxtimes - \frac{\pi}{12}\frac{1}{r} + \sigma r + \frac{\boxminus}{r^2}$ for $8 \leq \frac{r}{a} \leq 10$
- 3 parameters: $V(r) = \boxtimes - \frac{\boxplus}{r} + \sigma r$ for $6 \leq \frac{r}{a} \leq 10$
- 4 parameters: $V(r) = \boxtimes - \frac{\pi}{12}\frac{1}{r} + \sigma r + \frac{\boxminus}{r^2} + \frac{\boxplus}{r^3} + \frac{\boxdot}{r^4}$ for $4 \leq \frac{r}{a} \leq 10$

Note the phenomenological values $\frac{\pi}{12}$ for the coupling (*Lüscher Term* [25]) and $\sigma = \sigma_{fix}$ (cf. equation (4.16)). Symbols like $\boxminus$ and $\boxtimes$ stand for the fitting parameters. The choice of the fit model in position space causes a systematic error $\Delta_{fit}$ for $\Lambda_{\overline{MS}}$. This error must be considered in the final result. Unless explicitly specified otherwise the following fits will be applied to a data set that was generated by modelling based on a 4-parameter fit.

### 5.2.2. Variation of the fit formulae in momentum space

In chapter 2 different perturabtive expressions for the perturbative potential are presented. Fitting those expressions to the lattice values yields $\Lambda_{\overline{MS}}$. One gets $\Lambda_{\overline{MS}}$ either by determination of the coupling $\alpha_s(\mu)$ and insertion of its value to the formula (cf. equations (2.16, 2.17)) or by a direct fit to the data (cf. equation (2.18)). Furthermore in equation (2.18) one can set $\mu = p$. The different fit formulae are labelled as follows:

**A** : $\Lambda_{\overline{MS}}$ in MeV according to eq. (2.16)

**B** : $\Lambda_{\overline{MS}}$ in MeV according to eq. (2.17)

**C** : $\Lambda_{\overline{MS}}$ in MeV according to eq. (2.18)

**D** : $\Lambda_{\overline{MS}}$ in MeV according to eq. (2.18) with $\mu = p$

### 5.2.3. Variation of input parameters

In formula **A**, **B** and **C** the input parameters for the fitting procedure are the lower border of the momentum space fit range $p_{min}$, its upper border $p_{max}$ and the scale $\mu$. For formula **D** the input parameters simply consist of $p_{min}$ and $p_{max}$.

The input parameters take the following values:

- $1000\text{MeV} \leq p_{min} \leq 1750\text{MeV}$
- $1750\text{MeV} \leq p_{max} \leq 2500\text{MeV}$
- $\mu = \frac{p_{min}+p_{max}}{2}$

In the range of 1000MeV...2500MeV the perturbation theory is expected to be quite reliable, since $\alpha_s(\mu) \lesssim 0.3$.

All investigations are performed for the finest lattice spacing according to $\beta = 4.35$ (cf. table 4.1) on a lattice of $(\frac{L}{a})^3 = (256)^3$.

To exemplify the fitting procedure to lattice data, the fits of the different perturbative orders are shown in figure 5.1.

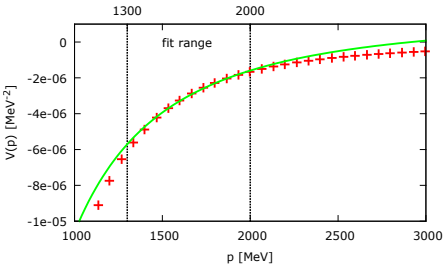


(a) LO - $\Lambda_{\overline{MS}} = 729(1)$MeV

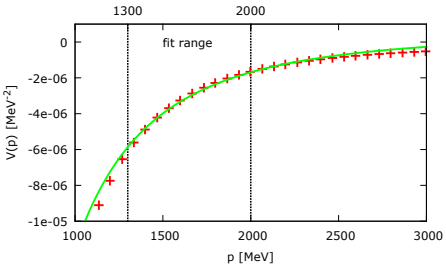


(b) NLO -$\Lambda_{\overline{MS}} = 548(2)$MeV

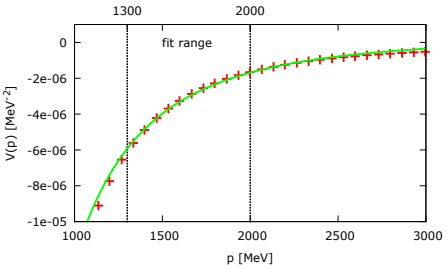


(c) NNLO - $\Lambda_{\overline{MS}} = 439(2)(1)$MeV

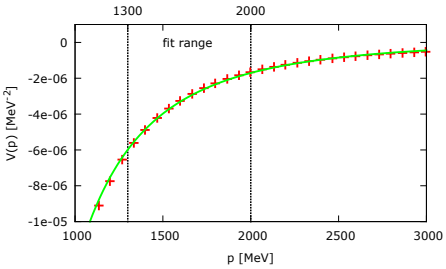


(d) NNNLO - $\Lambda_{\overline{MS}} = 383(1)$MeV

Figure 5.1.: Exemplary fits (formula **A**)

| | | 2 parameters | 3 parameters | 4 parameters |
|---|---|---|---|---|
| **A** | NNLO | 406...490 | 371...390 | 417...453 |
| | NNNLO | 352...427 | 327...337 | 362...394 |
| **B** | NNLO | 410...493 | 372...394 | 422...456 |
| | NNNLO | 354...429 | 328...340 | 365...399 |
| **C** | NNLO | 399...438 | 367...383 | 410...448 |
| | NNNLO | 346...422 | 324...333 | 357...393 |
| **D** | NNLO | 338...425 | 324...331 | 351...396 |
| | NNNLO | 309...390 | 296...306 | 320...364 |

Table 5.1.: Results for $\Lambda_{\overline{MS}}$ [MeV]: different fit models in position space (results for NNLO and NNNLO)

For a first impression $\alpha_s(\mu)$ is determined by a fit of the different orders of (2.3) to the lattice data. The figures are labelled by the corresponding results for $\Lambda_{\overline{MS}}$ which are determined by insertion of the respective $\alpha_s(\mu)$ value to **A**.

To determine the systematic error from the choice of the fit model in position space, one must consider the different results for $\Lambda_{\overline{MS}}$. In figure 5.2 the results for $\Lambda_{\overline{MS}}$ for the different perturbative formula and a 2-parameter fit in position space can be found. In figure 5.3 a 3-parameter and in figure 5.4 a 4-parameter fit is applied. The fit range has a width of 700MeV in each case. The center of the fit range is plotted on the x-axis. In table 5.1 the numerical results for NNLO and NNNLO can be found.

As mentioned above the systematic error $\Delta_{fit}$ of the choice of the fit function in position space must be considered. The 2-parameter fit is not included in the error determination, since it appeared to be very sensitive to discontinuities in the lattice potential and is therefore not considered to yield precise results (cf. chapter 4). **C** and **D** as well as the NNLO results are not included, since the resulting values differ much from the other results. As the systematic uncertainty the average deviation between the NNNLO result for $\Lambda_{\overline{MS}}$ from the 3-parameter fit

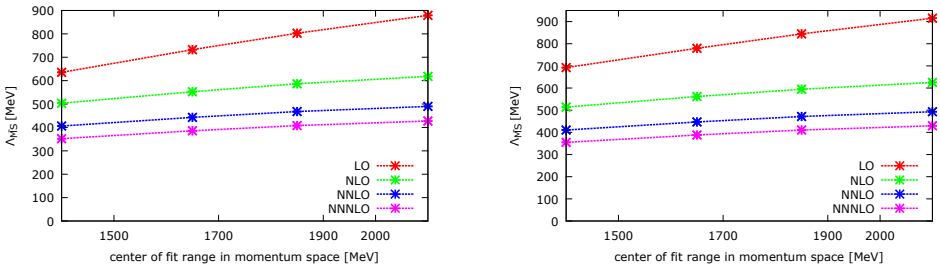


(a) formula **A**




(b) formula **B**

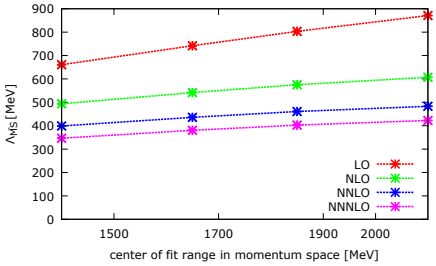


(c) formula **C**

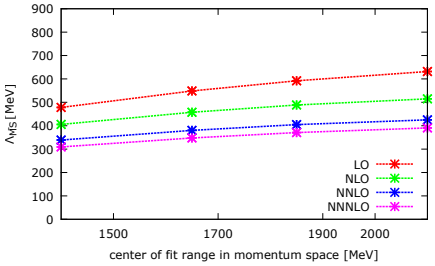


(d) formula **D**

Figure 5.2.: $\Lambda_{\overline{MS}}$ by a fit of different perturbative formulae in different orders on data based on extrapolation with a 2-parameter fit in position space (fit range width=1000 MeV)

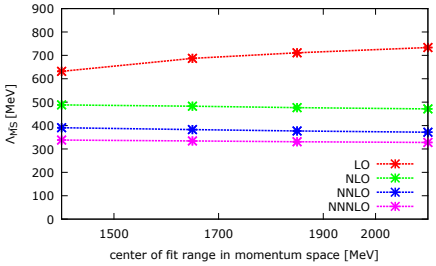


(a) formula **A**

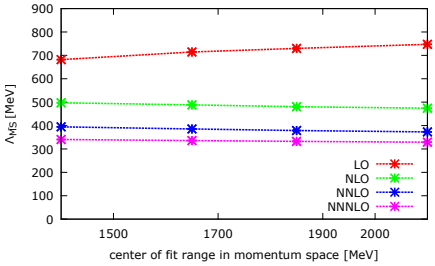


(b) formula **B**

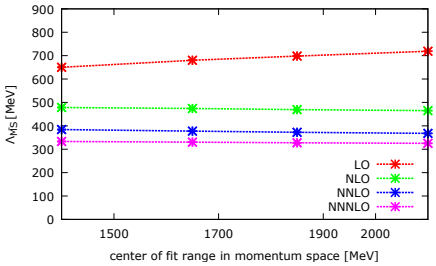


(c) formula **C**

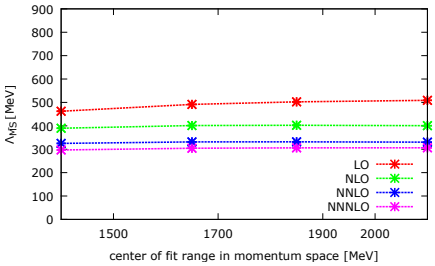


(d) formula **D**

Figure 5.3.: $\Lambda_{\overline{MS}}$ by a fit of different perturbative formulae in different orders on data based on extrapolation with a 3-parameter fit in position space (fit range width=700 MeV)

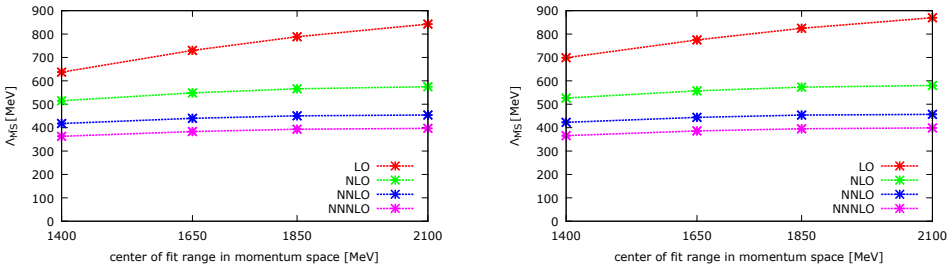


(a) formula **A**




(b) formula **B**

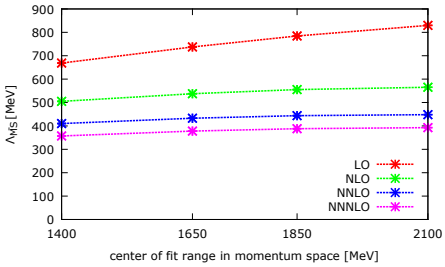


(c) formula **C**

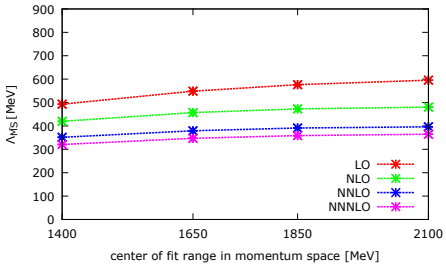


(d) formula **D**

Figure 5.4.: $\Lambda_{\overline{MS}}$ by a fit of different perturbative formulae in different orders on data based on extrapolation with a 4-parameter fit in position space (fit range width=700 MeV)

and the 4-parameter fit for **A** and **B** is considered (cf. table 5.1):

$$\Delta_{fit} = 47\text{MeV} \tag{5.2}$$

Another source of systematic error is given by the width of the fit range in momentum space. Therefore, the fit range is varied to $p_{max} - p_{min} = 1000$MeV. The results are shown in figure 5.5. On the horizontal axis the center of the fit range is shown. For data modelling in position space a 4-parameter is applied. For the fit range width of 1000MeV for different perturbative expressions one finds the results for $\Lambda_{\overline{MS}}$ for NNLO and NNNLO in table 5.2. For easier comparison with the fit range width of 700MeV the 4-parameter data from table 5.1 is reproduced.

| | | $p_{max} - p_{min} = 1000$MeV | $p_{max} - p_{min} = 700$MeV |
|---|---|---|---|
| **A** | NNLO | 426...455 | 417...453 |
| | NNNLO | 371...397 | 362...394 |
| **B** | NNLO | 430...458 | 422...456 |
| | NNNLO | 374...399 | 365...399 |
| **C** | NNLO | 419...449 | 410...448 |
| | NNNLO | 366...393 | 357...393 |
| **D** | NNLO | 325...392 | 351...396 |
| | NNNLO | 328...360 | 320...364 |

Table 5.2.: Results for $\Lambda_{\overline{MS}}$ [MeV] for different fit range widths in momentum space (results for NNLO and NNNLO)

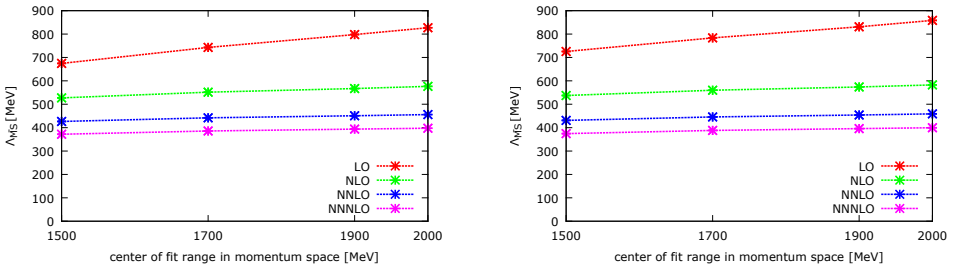


(a) formula **A**




(b) formula **B**

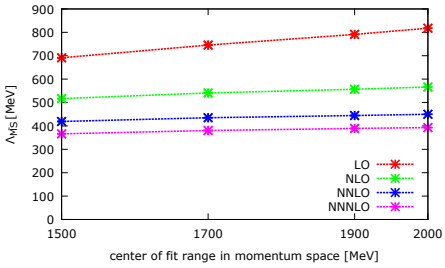


(c) formula **C**

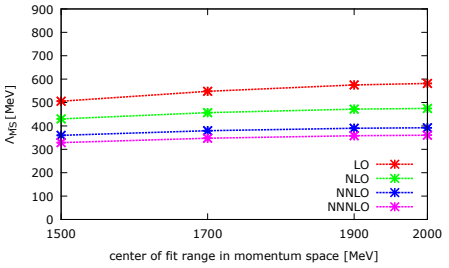


(d) formula **D**

Figure 5.5.: $\Lambda_{\overline{MS}}$ by a fit of different perturbative formulae in different orders on data based on extrapolation with a 4-parameter fit in position space (fit range width=1000 MeV)

In LO and NLO the results for $\Lambda_{\overline{MS}}$ differ much from those for NNLO and NNNLO (cf. figures 5.2, 5.3, 5.4 and 5.5). Also the results for expressions **C** and **D** differ significantly from those for **A** and **B**, even for NNLO and NNNLO[1]. The reason is, that in the derivation of the perturbation theory formula **C** respectively **D** in comparison to **A** and **B** one more approximation is applied (cf. equation (2.18)). For further analysis this formula is less appropriate since there is no reason for using an imprecise formula if there is a better one. However, the differences of the results of **A** and *B*, respectively **C** and **D** show, that perturbation theory works well, since a more precise formula yields a more precise result than a less precise formula. On the other hand, as expected, expressions **A** and **B** yield similar results. For further analysis the two higher orders will be the proper choice.

### 5.2.4. The systematic error of the fitting procedure

A large number of fits with input parameters randomly chosen is performed. The intervals for the random choice of the input parameters are:

- $p_{min}$ in 1000MeV...1750MeV
- $p_{max}$ in 1750MeV...2500MeV
- $\mu$ in $p_{min}...p_{max}$

To ensure a fit range that is large enough to contain as many values to perform a fit reasonably, the demand on the parameters is to form a fit range which measures at least a quarter of the maximally possible range:

[1] Moreover the difference between the results from **C** and **D** seem alarming at first glance: The choice of $\mu = p$ should not yield large deviations since, as stated in chapter 2, $\mu$ can be chosen arbitrarily. But there is an explanation for the derivation: The choice of a fixed value of $\mu$ is better suited for the considered momentum range than the choice of $\mu = p$ because of intrinsic properties of the perturbative formulae. In the considered momentum range the choice of a fixed $\mu$ is justified [26].

$$p_{max} - p_{min} \geq \frac{2500\text{MeV} - 1000\text{MeV}}{4} = 375\text{MeV} \tag{5.3}$$

The following fits are performed:

- expression **A**: 10,000 NNLO fits, 10,000 NNNLO fits
- expression **B**: 10,000 NNLO fits, 10,000 NNNLO fits

For the data modelling in position space a 4-parameter fit is applied. For the 40,000 values mean and standard derivative are derived. The standard derivative is taken as systematic error $\Delta_{syst}$.

As a result, one finds:

$$\Lambda_{\overline{MS}} = 417(41)\text{MeV} \tag{5.4}$$

Notice that the Jackknife error on the individual result for $\Lambda_{\overline{MS}}$ is about 1MeV. Therefore it is negligible compared to the standard derivative.

To show that it is possible to produce a result which is in agreement with the result from [3], the same procedure is performed again with application of a 3-parameter fit in position space, a limitation of the fit range width to 700MeV and with respect to NNNLO results exclusively.

The result is:

$$\Lambda_{\overline{MS}}^{\text{NNNLO}} = 331(11)\text{MeV} \tag{5.5}$$

It is consistent with the result determined earlier in this section within a $2\Delta_{fit}$-error range.

## 5.3. Systematic errors from the lattice computation

In the following systematic errors from the lattice computation are analysed.

### 5.3.1. Lattice discretization errors

First the lattice discretization error is analysed. There are four lattice ensembles available (cf. table 4.1). The fit range in position space is kept constant in physical units as far as possible[2]. The fit range in momentum space is kept constant at 1300MeV...2000MeV. The choice of $\mu$ is: $\mu = \frac{1300\text{MeV}+2000\text{MeV}}{2}$. The NNNLO fit for **A** is considered.

For the fit model $V(r) = \boxtimes - \frac{\pi}{12}\frac{1}{r} + \sigma r + \frac{\boxminus}{r^2} + \frac{\boxplus}{r^3} + \frac{\boxdot}{r^4}$ fit ranges and results are (cf. figure 5.6):

$\beta = 4.35 \ : \ 4.0a...10.0a \Rightarrow \Lambda_{\overline{MS}} = 383(16)\text{MeV}$

$\beta = 4.20 \ : \ 3.3a...8.2a \Rightarrow \Lambda_{\overline{MS}} = 366(12)\text{MeV}$

$\beta = 4.05 \ : \ 2.7a...6.7a \Rightarrow \Lambda_{\overline{MS}} = 381(24)\text{MeV}$

$\beta = 3.90 \ : \ 3.2a...5.6a \Rightarrow \Lambda_{\overline{MS}} = 408(37)\text{MeV}$

The error is the quadratic sum of the Jackknife error and the lattice spacing error (cf. table 4.1).

The extrapolation to $a \to 0$ is done by a linear fit to the four data points assuming a dependence of $a^2$.

The slope of the fitted line is very small, which causes for example the difference between the central values of $\Lambda_{\overline{MS}}$ for the finest lattice spacing and the continuum extrapolation to be less than 1MeV. The uncertainty caused by the lattice discretization can be neglected in the further analysis.

[2] In the case of $\beta = 3.90$ an enlargement of the fit range is necessary to ensure that $\frac{\chi^2}{\text{dof}} \leq 1$

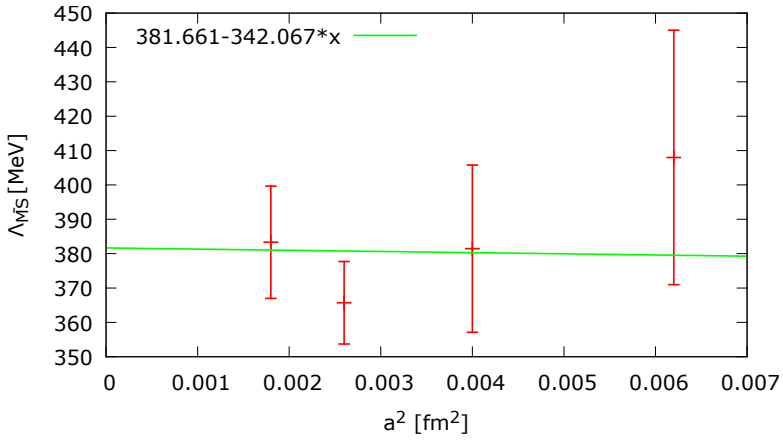


Figure 5.6.: $\Lambda_{\overline{MS}}$ for different lattice spacings, 4-parameter fit in position space

### 5.3.2. Effects associated with $\frac{r_0}{a} = 9.81(13)$

Since the final result for $\Lambda_{\overline{MS}}$ is listed not only in MeV but also in units of $r_0$, the uncertainty on the Sommer parameter $\frac{r_0}{a} = 9.81(13)$ must be considered (cf. [3]).

### 5.3.3. Finite volume effects

As one could assume from section 4.2.1, the finite volume effects are very small. The variation of the result for $\Lambda_{\overline{MS}}$ smaller than 1MeV if the lattice extent is reduced to $N_s = 128$. Since the uncertainty is negligible compared to the systematic error determined in section 5.2.4, it will not be considered in the final result.

### 5.3.4. Non-vanishing light quark masses

The effect that in perturbation theory dynamical quarks are considered massless while lattice results use small finite quark masses has been investigated in [3]. The uncertainty was considered negligibly small. For this reason, no significant corrections from non-vanishing quark masses are expected in the present case. It will not be considered in the final result.

## 5.4. Final results for $\Lambda_{\overline{MS}}$

The final result for $\Lambda_{\overline{MS}}$ for $n_f = 2$ dynamical quark flavours based on lattice results for the finest available lattice spacing ($\beta = 4.25$) is stated in the following. The result is quoted in MeV as well as in units of $r_0$. The following errors are taken into account:

- The error associated with the choice of the fit model in position space $\Delta_{fit} = 47$MeV (cf. 5.2.3).
- The systematic error associated with the fitting procedure $\Delta_{syst} = 41$MeV (cf. section 5.2.4).
- The errors associated with $\frac{r_0}{a} = 9.81(13)$ and the lattice spacing $a = 0.0420(17)$ (cf. table 4.1)).

For the result in lattice units (respectively MeV) the error is calculated the following way:

$$\begin{aligned}\frac{\Lambda_{\overline{MS}}a}{a} &\to \frac{\Lambda_{\overline{MS}}a \pm \Delta_{fit}a \pm \Delta_{syst}a}{a \pm \Delta a} \\ &= \frac{\Lambda_{\overline{MS}}a \pm \Delta_{fit}a \pm \Delta_{syst}a}{a}\left(1 \pm \frac{\Delta a}{a}\right) + \mathcal{O}((\Delta a)^2) \\ &= \Lambda_{\overline{MS}} \pm \underbrace{\frac{\Delta_{fit}a \pm \Delta_{syst}a}{a}}_{\text{error on } \Lambda_{\overline{\text{MS}}}} \pm \underbrace{\frac{\Lambda_{\overline{MS}}a\Delta a}{a^2}}_{\text{lattice spacing error}} + \mathcal{O}((\Delta a)^2)\end{aligned} \tag{5.6}$$

Since they are all independent, the error on $\Lambda_{\overline{MS}}$ as well as the lattice spacing error are added quadratically:

$$\Delta = \sqrt{\left(\frac{\Lambda_{\overline{MS}}a\Delta a}{a^2}\right)^2 + (\Delta_{fit})^2 + (\Delta_{syst})^2} \tag{5.7}$$

For the result in units of $r_0$ the calculation works analogous:

$$\Lambda_{\overline{MS}}a\frac{r_0}{a} \to (\Lambda_{\overline{MS}}a \pm \Delta_{fit}a \pm \Delta_{syst}a)\left(\frac{r_0}{a} \pm \Delta\frac{r_0}{a}\right) \tag{5.8}$$

One finds:

$$\Lambda_{\overline{MS}} = 417(64)\text{MeV} \qquad \text{respectively} \qquad \Lambda_{\overline{MS}}r_0 = 0.87(13) \tag{5.9}$$

Compare to the results determined in [3]:

$$\Lambda_{\overline{MS}} = 315(30)\text{MeV} \qquad \text{respectively} \qquad \Lambda_{\overline{MS}}r_0 = 0.658(55) \tag{5.10}$$

The result determined in this work differs significantly from the one determined in 2011. Moreover, its uncertainty is even larger.

# 6. Conclusion and outlook

The result for $\Lambda_{\overline{MS}}$ determined in this work is not in accordance with the result from 2011 [3]. The error could not be reduced but is even larger than in the preliminary work. On the one hand, the a priory promising approach of a determination of $\Lambda_{\overline{MS}}$ in momentum space has not kept its promise. To avoid the error that occurs during a Fourier transform of perturbative results to position space by transforming lattice data to momentum space is not sufficient.
Conversely, the transformation of lattice data holds further difficulties. One of the most important sources of uncertainty is the fitting procedure in position space. The investigation in position space did not require such a procedure, so the associated uncertainty was not considered. The error determined in position space might be underestimated. Lattice data turned out to be very sensitive to the choice of the fit model to model data at large distances. In the beginning of the investigations presented in this work the assumption was that the modelled part of the lattice data would not play a crucial role for the overall result. The results presented in table 5.1 show the very reverse: A different choice of the fit model in position space affects the result remarkably. Also the wiggly behaviour of the potential in momentum space presented in section 4.3 occurs because of the extrapolation procedure. Briefly, the difficulties associated with the large distances respectively small momenta that were observed in 2011 appear again.

One probably needs precise lattice results at large distances to reduce those difficulties.
Moreover the fitting procedure in momentum space influences the result. As one can see in section 5.2.4 the result from 2011 can almost be reproduced by a choice of the proper parameters. But there is no reason to prefer a certain parameter setup. This might indicate again that the systematic errors in 2011 have been underestimated.

On the other hand, the differing result might have uncovered possible areas for improvement. A final judgement on the quality of the result cannot be formed yet. The problem is, that objects in momentum space are affected by the entire setup in position space and vice versa.

There is no exact mapping of the choice of the parameters in position space to the parameters in momentum space. So the comparison of momentum space and position space results is highly non-trivial and has to be studied in more detail. Future investigations should inquire the relation of momentum and position space further.

# A. Perturbative coefficients

The coefficients that occur in expressions associated with the quark-antiquark potential read [9]:

$$P_1(L) = a_1 + \beta_0 L \tag{A.1}$$
$$P_2(L) = a_2 + (2a_1\beta_0 + \beta_1)\, L + \beta_0^2 L^2 \tag{A.2}$$
$$P_3(L) = a_3 + (3a_2\beta_0 + 2a_1\beta_1 + \beta_2)L + \beta_0 \left(3a_1\beta_0 + \frac{5}{2}\beta_1\right) L^2 + \beta_0^3 L^3 \tag{A.3}$$

where [27]

$$\beta_0 = 11 - \frac{2}{3}n_f \tag{A.4}$$
$$\beta_1 = 102 - \frac{38}{3}n_f \tag{A.5}$$
$$\beta_2 = \frac{2857}{2} - \frac{5033}{18}n_f + \frac{325}{54}n_f^2 \tag{A.6}$$
$$\beta_3 = \left(\frac{149753}{6} + 3564\zeta(3)\right) - \left(\frac{1078361}{162} + \frac{6508}{27}\zeta(3)\right) n_f + \left(\frac{50065}{162} + \frac{6472}{81}\right) n_f^2 + \frac{1093}{729}n_f^3 \tag{A.7}$$

Further [6, 7, 28]

$$a_1 = \frac{31}{3} - \frac{10}{9}n_f \tag{A.8}$$
$$a_2 = \left(\frac{4343}{18} + 36\pi^2 - \frac{9}{4}\pi^4 + 55\zeta(3)\right) - \left(\frac{1229}{27} + \frac{52}{3}\zeta(3)\right) n_f + \frac{100}{81}n_f^2 \tag{A.9}$$
$$a_3 = \overline{a}_3 + 144\pi^2 \left(\ln 3 + \gamma_E - \frac{5}{6}\right) \tag{A.10}$$
$$a_{3\,\ln} = 144\pi^2 \tag{A.11}$$

with $\gamma_E$ the Euler–Masceroni constant and

$$\overline{a}_3 = a_3^{(0)} + a_3^{(1)} n_f + a_3^{(2)} n_f^2 + a_3^{(3)} n_f^3 \tag{A.12}$$

where

$$a_3^{(0)} = 27c_1 + \frac{15}{1}c_2 \tag{A.13}$$
$$a_3^{(1)} = \frac{9}{2}c_3 \frac{5}{96}c_4 - \frac{68993}{81} + \frac{16624}{27}\zeta(3) + \frac{160}{9}\zeta(5) \tag{A.14}$$
$$a_3^{(2)} = \frac{93631}{972} + \frac{16}{45}\pi^4 + \frac{412}{9}\zeta(3) \tag{A.15}$$
$$a_3^{(3)} = -\frac{1000}{729} \tag{A.16}$$

and [6, 7]

$$c_1 = 502.24(1) \tag{A.17}$$
$$c_2 = -136.39(12) \tag{A.18}$$
$$c_3 = -709.717 \tag{A.19}$$
$$c_4 = -56.83(1) \tag{A.20}$$

# B. Data modelling code

The modelling of lattice data is basically a spherically symmetric problem. In the following is assumed that the data is given in a table form with four columns:

| $x$ | $y$ | $z$ | $V(r)$ |
|---|---|---|---|
| ... | ... | ... | ... |

Because the potential $V(r)$ is symmetric it is enough to consider $r$-values given by $r = \sqrt{x^2 + y^2 + z^2}$ with $z \leq y \leq x$. The quantities come in lattice units. The lattice data is stored in the arrays inputX[ ], inputY[ ], inputZ[ ] and inputV[ ]. The extrapolation processes in two steps. First a $\chi^2$-minimizing fit[1] is applied to data within a fit range $r_{min} \leq r \leq r_{max}$. With the obtained fit-function a 3-dimensional array V[L][L][L] is filled, L is the chosen lattice extend.

Listing B.1: Initialization with fit-function

```
// initialize a cubic lattice with fit-function V(r)

for(i1 = 0; i1 < L; i1++){
        for(i2 = 0; i2 < L; i2++){
                for(i3 = 0; i3 < L; i3++){
                        V[i1][i2][i3] = 0.0;

                        if(i1 != 0 || i2 != 0 || i3 != 0){
                                double x = (double)i1;
                                if(i1 > L/2)
                                        x = (double)(L-i1);
                                double y = (double)i2;
                                if(i2 > L/2)
                                        y = (double)(L-i2)
                                double z = (double)i3;
                                if(i3 > L/2)
                                        z = (double)(L-i3);

                                double r = sqrt(x*x + y*y + z*z);

                                V[i1][i2][i3] =  <FIT FUNCTION (r)>;

                        }
                }
        }
}
```

The second step is to replace those entries of the array for which values are available by real lattice data. The following C++ code fragment shows the replacement algorithm.

Listing B.2: Replacement by lattice values

```
for(i1 = 0; i1 < inputX.size(); i1++){
        if(inputX[i1] > L/2)
                continue;
        if(inputY[i1] > L/2)
                continue;
        if(inputZ[i1] > L/2)
```

[1] Realized using the GNU Scientific Library (GSL) which provides programming tools for numerical applications in C/C++ (cf. `http://www.gnu.org/software/gsl/`).

```
                continue;

        double V_ = inputV[i1];

        // permute x, y, z:
        for(i2 = 0; i2 < 6; i2++){
                int x_, y_, z_;

                if(i2 == 0){
                        x_ = input_x_[i1];
                        y_ = input_y_[i1];
                        z_ = input_z_[i1];
                }
                if(i2 == 1){
                        x_ = input_z_[i1];
                        y_ = input_x_[i1];
                        z_ = input_y_[i1];
                }
                if(i2 == 2){
                        x_ = input_y_[i1];
                        y_ = input_z_[i1];
                        z_ = input_x_[i1];
                }
                if(i2 == 3){
                        x_ = input_z_[i1];
                        y_ = input_y_[i1];
                        z_ = input_x_[i1];
                }
                if(i2 == 4){
                        x_ = input_x_[i1];
                        y_ = input_z_[i1];
                        z_ = input_y_[i1];
                }
                if(i2 == 5){
                        x_ = input_y_[i1];
                        y_ = input_x_[i1];
                        z_ = input_z_[i1];
                }

                // the eight regions +/-x, +/-y, +/-z:
                for(i3 = 0; i3 < 8; i3++){
                        int x__, y__, z__;

                        if(i3 == 0){
                                x__ = x_;
                                y__ = y_;
                                z__ = z_;
                        }
                        if(i3 == 1){
                                x__ = (L_-x_)%L_;
                                y__ = y_;
                                z__ = z_;
                        }
                        if(i3 == 2){
                                x__ = x_;
                                y__ = (L_-y_)%L_;
                                z__ = z_;
                        }
                        if(i3 == 3){
                                x__ = x_;
                                y__ = y_;
                                z__ = (L_-z_)%L_;
                        }
                        if(i3 == 4){
                                x__ = x_;
                                y__ = (L_-y_)%L_;
                                z__ = (L_-z_)%L_;
```

```
                        }
                        if(i3 == 5){
                                x__ = (L_-x_)%L_;
                                y__ = y_;
                                z__ = (L_-z_)%L_;
                        }
                        if(i3 == 6){
                                x__ = (L_-x_)%L_;
                                y__ = (L_-y_)%L_;
                                z__ = z_;
                        }
                        if(i3 == 7){
                                x__ = (L_-x_)%L_;
                                y__ = (L_-y_)%L_;
                                z__ = (L_-z_)%L_;
                        }

                        V[x__][y__][z__] = V_;
                }
        }
}
```

# C. Symanzik improvement

A new position space technique allows to compute several complicated integrals more precisely than with the standard Monte Carlo integration [29].

Consider first the 4d-case: Let the interaction only contain diagrams with free propagators $\sim \frac{1}{\hat{p}^2}$ on a 4d lattice $\Lambda_4$ and lattice spacing $a = 1$. The momentum is

$$p = (p_0, .., p_3) \quad \text{and} \quad \hat{p}_\mu = 2 \sin\left(\frac{1}{2} p_\mu\right) \tag{C.1}$$

This scenario describes the case of pure gauge theory with standard Wilson action. As an example look at the following integral:

$$A_0 = \int_{-\pi}^{+\pi} \frac{d^4k}{(2\pi)^4} \frac{d^4q}{(2\pi)^4} \frac{1}{\hat{k}^2 \hat{q}^2 (-\hat{k}^2 - \hat{q})^2} \tag{C.2}$$

Now the position space operator is introduced:

$$G(x) = \int_{-\pi}^{+\pi} \frac{d^4p}{(2\pi)^4} \frac{e^{ipx}}{\hat{p}^2} \tag{C.3}$$

Perform the sum over the hypercube $\Lambda_4$ and verify that:

$$A_0 = \sum_{x \in \Lambda_4} G(x)^3 \tag{C.4}$$

$G(x)$ is a propagator, so:

$$-\triangle G(x) = \begin{cases} 1 & \text{if} \quad x = 0 \\ 0 & \text{otherwise} \end{cases} \tag{C.5}$$

One observes:

$$x_\mu H(x) = (\nabla^*_\mu + \nabla_\mu) G(x) \qquad \text{with} \quad H(x) = \int_{-\pi}^{+\pi} \frac{d^4p}{(2\pi)^4} e^{ipx} \ln \hat{p}^2 \tag{C.6}$$

with the definition of the derivatives

$$\nabla_\mu f(x) = f(x + \hat{\mu}) - f(x), \qquad \nabla^*_\mu f(x) = f(x) - f(x - \hat{\mu}) \tag{C.7}$$

$\hat{\mu}$ is the unit vector in $\mu$-direction, one finds by summing equation (C.6) over $\mu$:

$$H(x) = \frac{2}{\rho} \sum_\mu (G(x) - G(x - \hat{\mu})), \qquad \rho = \sum_\mu x_\mu \tag{C.8}$$

With (C.7) one finds a recursive equation for the lattice operator:

$$\boxed{G(x + \hat{\mu}) = G(x - \hat{\mu}) + x_\mu H(x) = G(x - \hat{\mu}) + \frac{2x_\mu}{\rho} \sum_\mu (G(x) - G(x - \hat{\mu}))} \tag{C.9}$$

so one can express $G(x)$ as an equation of the values: $G(0,0,0,0)$, $G(1,0,0,0)$,.., $G(1,1,1,1)$.

For the improvement of the static quark-antiquark potential (in [3] for an, the 3d-application has to be used. The Symanzik action is considered.

On the lattice, the force between two quarks can be expressed by

$$F(r_I) = \frac{V(r) - V(r-a)}{a} \tag{C.10}$$

$r_I$ is the distance at which the force has no deviations from the force in the continuum when it is evaluated on tree-level. One says $F(r_I)$ is a tree-level improved observable.

Following [30] the force is:

$$\begin{aligned} F_{tree}(r') &= \frac{V_{tree}(r) - V_{tree}(r-a)}{a} \\ &= -\frac{4}{3} g_0^2 [G(r,0,0) - G(r-a,0,0)] \end{aligned} \tag{C.11}$$

with $G(\vec{r}) = \frac{1}{a}\int_{-\pi}^{+\pi} \frac{d^3k}{(2\pi)^3} \frac{\prod_j \cos(\frac{x_j k j 1}{a})}{4\sum_j \sin^2(\frac{k_j}{2})}$ the 3d-lattice propagator.

In short, the tree-level improved force is:

$$\boxed{F(r_I) = \frac{4}{3}\frac{g_0^2}{4\pi r_I^2} + \mathcal{O}(g_0^4), \qquad \frac{1}{4\pi r_I^2} = -\frac{G(r,0,0) - G(r-1,0,0)}{a}} \tag{C.12}$$

And the tree-level improved potential is:

$$\boxed{\frac{1}{4\pi r_I} = G(\vec{r})} \tag{C.13}$$

Only the $\mathcal{O}(g_0^4)$-part contains lattice artefacts.

The theory about this improvement that explains how to handle lattice artefacts is Symanzik's effective theory.

By solving the recursive equation in 3d

$$\boxed{G(x+\hat{j}) = G(x-\hat{j}) + \frac{2x_j}{\rho}\sum_i (G(x) - G(x-\hat{i}))} \tag{C.14}$$

$x = (x_1, x_2, x_3)$, $\hat{j}$ is the unit vector in j-direction, $j = 1, 2, 3$. Because of the isotropy of $G(x)$, it is enough to consider the case $x_1 \geq x_2 \geq x_3$.

In order to compare physical potential and Coulomb potential, the propagator

$$G(\vec{r}) = \int_{-\pi}^{+\pi} \frac{d^3k}{(2\pi)^3} \frac{\prod_j \cos(r_j k_j)}{4\left(\sum_j \sin^2\left(\frac{k_j}{2}\right) + \frac{4}{3}\sum_j \sin^4\left(\frac{k_j}{2}\right)\right)} \tag{C.15}$$

has to be computed [3]. To avoid large statistical errors because of the singularity at $\vec{k} = 0$ one can split the integral:

$$G(\vec{r}) = G_1(\vec{r}) + G_2(\vec{r}) \tag{C.16}$$

with

$$G_1(\vec{r}) = \int_{-\pi}^{+\pi} \frac{d^3k}{(2\pi)^3} \frac{\prod_j \cos(r_j k_j)}{4\left(\sum_j \sin^2\left(\frac{k_j}{2}\right)\right)} \tag{C.17}$$

and

$$G_2(\vec{r}) = \int_{-\pi}^{+\pi} \left( \frac{d^3k}{(2\pi)^3} \frac{\prod_j \cos(r_j k_j)}{4\left(\sum_j \sin^2\left(\frac{k_j}{2}\right) + \frac{4}{3}\sum_j \sin^4\left(\frac{k_j}{2}\right)\right)} - \frac{\prod_j \cos(r_j k_j)}{4\left(\sum_j \sin^2\left(\frac{k_j}{2}\right)\right)} \right) \tag{C.18}$$

Because of numerical effects, computation of the propagator only makes sense in the region

$$r_I \leq r_{crit} \tag{C.19}$$

beyond the critical distance the numerical errors become too large and the value of $G(\vec{r})$ turns out to be nonphysical. The values $G(\vec{r})$ where $|\vec{r}| \geq r_{crit}$ are extrapolated by $\frac{1}{4\pi r}$.

In this work, the investigation is performed in momentum space. So in a next step, the propagator values are discretely Fourier-transformed. Afterwards, those values and the analytical formula

$$\tilde{V}(p) = \frac{1}{p^2} \tag{C.20}$$

are matched. In the case of matching, according to (C.13) the new momenta are found.

The last step is to compare analytical and propagator values for each point $p$ in momentum space. The shifts for each point are stored (cf. table C.1).

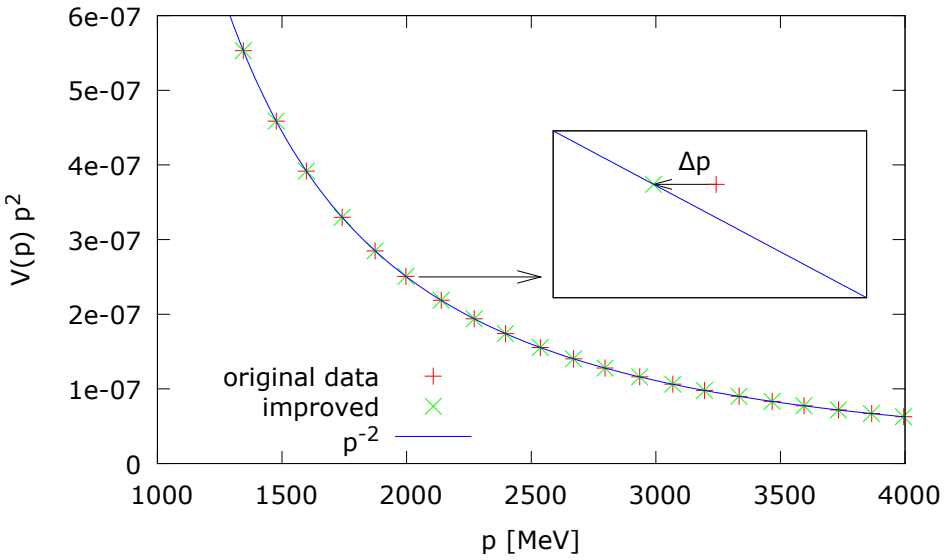


Figure C.1.: The propagator values are shifted to the analytical curve

For the improvement of lattice data, shifts are added to each data point according to table C.2. The procedure shifts the propagator values to the $\frac{1}{p^2}$-curve (cf. figure C.1). The improvement is shown in figure (4.24).

| $p$ | shift |
|---|---|
| $p_1$ | $\Delta p_1$ |
| $p_2$ | $\Delta p_2$ |
| $p_3$ | $\Delta p_3$ |
| $\dots$ | $\dots$ |

Table C.1.: Storage of shifts

| $p$ | potential value | new $p$ | improved potential |
|---|---|---|---|
| $p_1$ | $\tilde{V}(p_1)$ | $p_1 + \Delta p_1$ | $\tilde{V}(p_1) = \tilde{V}^{improved}(p_1 + \Delta p_1)$ |
| $p_2$ | $\tilde{V}(p_2)$ | $p_2 + \Delta p_2$ | $\tilde{V}(p_2) = \tilde{V}^{improved}(p_2 + \Delta p_2)$ |
| $p_3$ | $\tilde{V}(p_3)$ | $p_3 + \Delta p_3$ | $\tilde{V}(p_3) = \tilde{V}^{improved}(p_3 + \Delta p_3)$ |
| $\dots$ | $\dots$ | | |

Table C.2.: Assignment of new momenta

# Bibliography


[1] Kenneth G. Wilson. Confinement of quarks. *Phys. Rev. D*, 10:2445–2459, Oct 1974.

[2] M. Göckeler, R. Horsley, A. C. Irving, D. Pleiter, P. E. L. Rakow, G. Schierholz, and H. Stüben. Determination of the lambda parameter from full lattice qcd. *Phys. Rev. D*, 73:014513, Jan 2006.

[3] Karl Jansen, Felix Karbstein, Attila Nagy, and Marc Wagner. $\Lambda_{\bar{M}S}$ from the static potential for QCD with $n_f = 2$ dynamical quark flavors. *JHEP*, 1201:025, 2012.

[4] William A. Bardeen, A. J. Buras, D. W. Duke, and T. Muta. Deep-inelastic scattering beyond the leading order in asymptotically free gauge theories. *Phys. Rev. D*, 18:3998–4017, Dec 1978.

[5] Felix Karbstein. Quark-antiquark static energy from a restricted Fourier transform. 2013.

[6] Alexander V. Smirnov, Vladimir A. Smirnov, and Matthias Steinhauser. Three-loop static potential. *Phys.Rev.Lett.*, 104:112002, 2010.

[7] C. Anzai, Y. Kiyo, and Y. Sumino. Static QCD potential at three-loop order. *Phys.Rev.Lett.*, 104:112003, 2010.

[8] Thomas Appelquist, Michael Dine, and I. J. Muzinich. Static limit of quantum chromodynamics. *Phys. Rev. D*, 17:2074–2081, Apr 1978.

[9] F.A. Chishtie and V. Elias. RG / Pade estimate of the three loop contribution to the QCD static potential function. *Phys.Lett.*, B521:434–440, 2001.

[10] K.G. Chetyrkin, Bernd A. Kniehl, and M. Steinhauser. Strong coupling constant with flavor thresholds at four loops in the MS scheme. *Phys.Rev.Lett.*, 79:2184–2187, 1997.

[11] H. J. Rothe. *Lattice Gauge Theories - An Introduction.* World Scientific Lecture Notes in Physics - Vol. 59, 1997.

[12] P. Weisz. Continuum limit improved lattice action for pure yang-mills theory (i). *Nuclear Physics B*, 212(1):1 – 17, 1983.

[13] Roberto Frezzotti, Pietro Antonio Grassi, Stefan Sint, and Peter Weisz. Lattice QCD with a chirally twisted mass term. *JHEP*, 0108:058, 2001.

[14] Andrea Shindler. Twisted mass lattice QCD. *Phys.Rept.*, 461:37–110, 2008.

[15] R. Baron et al. Light hadrons from Nf=2+1+1 dynamical twisted mass fermions. *PoS*, LATTICE2010:123, 2010.

[16] Björn Fröhlich Wagenbach. *Numerische Berechnung des Quark-Antiquark-Potentials zur Bestimmung der kritischen Temperatur in der SU(2) Yang-Mills-Theorie.* Bachelor's Thesis, Goethe-Universität Frankfurt am Main, 2012.

[17] Michael Donnellan, Francesco Knechtli, Bjorn Leder, and Rainer Sommer. Determination of the Static Potential with Dynamical Fermions. *Nucl.Phys.*, B849:45–63, 2011.

[18] Frederic D.R. Bonnet, Patrick Fitzhenry, Derek B. Leinweber, Mark R. Stanford, and Anthony G. Williams. Calibration of smearing and cooling algorithms in SU(3): Color gauge theory. *Phys.Rev.*, D62:094509, 2000.

[19] R. Sommer. A New way to set the energy scale in lattice gauge theories and its applications to the static force and alpha-s in SU(2) Yang-Mills theory. *Nucl.Phys.*, B411:839–854, 1994.

[20] R. Baron, Ph. Boucaud, J. Carbonell, A. Deuzeman, V. Drach, et al. Light hadrons from lattice QCD with light (u,d), strange and charm dynamical quarks. *JHEP*, 1006:111, 2010.

[21] A. Sternbeck. *The infrared behavior of lattice QCD Green's functions.* PhD thesis, HU Berlin, 2006.

[22] Jeffrey E. Mandula. Gauge fixing on the lattice and the Gibbs phenomenon. 1998.

[23] J. Beringer et al. (Particle Data Group). *Phys. Rev. D86, 010001*, 2012.

[24] `http://www.physics.utah.edu/~detar/phycs6730/handouts/jackknife/jackknife/`.

[25] Martin Luscher. Lattice QCD: From quark confinement to asymptotic freedom. *Annales Henri Poincare*, 4:S197–S210, 2003.

[26] personal conversation with Felix Karbstein, 2014.

[27] T. van Ritbergen, J.A.M. Vermaseren, and S.A. Larin. The Four loop beta function in quantum chromodynamics. *Phys.Lett.*, B400:379–384, 1997.

[28] C. Anzai, Y. Kiyo, and Y. Sumino. Violation of Casimir Scaling for Static QCD Potential at Three-loop Order. *Nucl.Phys.*, B838:28–46, 2010.

[29] Martin Luscher and Peter Weisz. Coordinate space methods for the evaluation of Feynman diagrams in lattice field theories. *Nucl.Phys.*, B445:429–450, 1995.

[30] Silvia Necco and Rainer Sommer. The N(f) = 0 heavy quark potential from short to intermediate distances. *Nucl.Phys.*, B622:328–346, 2002.

# Acknowledgement

First of all I want to thank Marc Wagner for his patient and accurate supervision and for countless helpful discussions.

I would like to thank Felix Karbstein to bring me a deeper understanding of perturbation theory and for much valuable advice.

Thanks to Karl Jansen and Bartosz Kostrzewa for providing lattice computations and technical support.

# Selbstständigkeitserklärung

Hiermit versichere ich, dass ich die vorliegende Arbeit selbstständig verfasst und keine anderen als die angegebenen Quellen und Hilfsmittel benutzt habe, dass alle Stellen der Arbeit, die wörtlich oder sinngemäß aus anderen Quellen übernommen wurden, als solche kenntlich gemacht und dass die Arbeit in gleicher oder ähnlicher Form noch keiner anderen Prüfungsbehörde vorgelegt wurde.

Frankfurt am Main, den